Mannose-6-phosphate regulates destruction of lipid-linked oligosaccharides

Ningguo Gao[a,*], Jie Shang[a,*], Dang Huynh[b], Vijaya L. Manthati[b], Carolina Arias[c], Heather P. Harding[d], Randal J. Kaufman[e], Ian Mohr[c], David Ron[d], John R. Falck[a,b], and Mark A. Lehrman[a]

Departments of [a]Pharmacology and [b]Biochemistry, University of Texas Southwestern Medical Center at Dallas, Dallas, TX 75390; [c]Department of Microbiology, New York University School of Medicine, New York, NY 10016; [d]University of Cambridge Metabolic Research Laboratories, Cambridge CB2 0QQ, United Kingdom; [e]Departments of Internal Medicine and Biological Chemistry, University of Michigan Medical Center, Ann Arbor, MI 48109

ABSTRACT **Mannose-6-phosphate (M6P) is an essential precursor for mannosyl glycoconjugates, including lipid-linked oligosaccharides (LLO; glucose$_3$mannose$_9$GlcNAc$_2$-P-P-dolichol) used for protein *N*-glycosylation. In permeabilized mammalian cells, M6P also causes specific LLO cleavage. However, the context and purpose of this paradoxical reaction are unknown. In this study, we used intact mouse embryonic fibroblasts to show that endoplasmic reticulum (ER) stress elevates M6P concentrations, leading to cleavage of the LLO pyrophosphate linkage with recovery of its lipid and lumenal glycan components. We demonstrate that this M6P originates from glycogen, with glycogenolysis activated by the kinase domain of the stress sensor IRE1-α. The apparent futility of M6P causing destruction of its LLO product was resolved by experiments with another stress sensor, PKR-like ER kinase (PERK), which attenuates translation. PERK's reduction of *N*-glycoprotein synthesis (which consumes LLOs) stabilized steady-state LLO levels despite continuous LLO destruction. However, infection with herpes simplex virus 1, an *N*-glycoprotein-bearing pathogen that impairs PERK signaling, not only caused LLO destruction but depleted LLO levels as well. In conclusion, the common metabolite M6P is also part of a novel mammalian stress-signaling pathway, responding to viral stress by depleting host LLOs required for *N*-glycosylation of virus-associated polypeptides. Apparently conserved throughout evolution, LLO destruction may be a response to a variety of environmental stresses.**

Monitoring Editor
Reid Gilmore
University of Massachusetts

Received: Apr 14, 2011
Revised: Jun 8, 2011
Accepted: Jun 28, 2011

This article was published online ahead of print in MBoC in Press (http://www.molbiolcell.org/cgi/doi/10.1091/mbc.E11-04-0286) on July 7, 2011.

*Joint lead authors.

Address correspondence to: Mark A. Lehrman (mark.lehrman@utsouthwestern.edu).

Abbreviation used: AMAC, 2-aminoacridone; ANDS, 7-amino-1,3-naphthalenedisulfonic acid; AP, acceptor peptide; BSA, bovine serum albumin; CDG, congenital disorders of glycosylation; CHX, cycloheximide; DAB, 1,4-dideoxy-1,4-imino-D-arabinitol; Dol, dolichol; Dol-P, dolichol phosphate; DTT, dithiothreitol; ER, endoplasmic reticulum; ERAD, ER-associated degradation; F6P, fructose-6-phosphate; FACE, fluorophore-assisted carbohydrate electrophoresis; FBS, fetal bovine serum; G1P, glucose-1-P; $G_3M_9Gn_2$-P-P-Dol, glucose$_3$mannose$_9$*N*-acetylglucosamine$_2$-P-P-dolichol; G6P, glucose-6-phosphate; gC, representative glycoprotein; gCiGP, glycogen phosphorylase; h.p.i., hours postinfection; HSV-1, herpes simplex virus 1; IRE1, inositol-requiring enzyme 1; LLO, lipid-linked oligosaccharide; M1P, mannose-1-phosphate; M6P, mannose-6-phosphate; M6Po, mannose-6-phosphonate; MEF, mouse embryonic fibroblast; OT, oligosaccharyltransferase; PERK, PKR-like ER kinase; siRNA, small interfering RNA; SLO, streptolysin-O; TBS, Tris-buffered saline; TG, thapsigargin; TN, tunicamycin; UPR, unfolded protein response.

INTRODUCTION

An essential function of the eukaryotic endoplasmic reticulum (ER) is asparagine-linked (*N*-linked) glycosylation of nascent ER polypeptides. In the ER, *N*-linked glycans on the newly synthesized glycoproteins are processed by specific ER-associated glycosidases. The various processed glycans then interact with important ER-resident glycan-binding proteins (lectins) involved in protein folding, assembly, quality control, and, if necessary ER-associated degradation (ERAD). *N*-linked glycosylation absolutely requires the synthesis of a lipid-linked oligosaccharide (LLO) bearing a 14-sugar glycan in pyrophosphate linkage to dolichol (Dol), glucose$_3$mannose$_9$GlcNAc$_2$-P-P-dolichol ($G_3M_9Gn_2$-P-P-Dol; Figure 1). The LLO is utilized by the multi-subunit enzyme oligosaccharyltransferase (OT) for transfer of $G_3M_9Gn_2$ glycans to selected asparagine residues within the context Asn-X-Ser/Thr on newly synthesized polypeptide chains within the ER lumen. An LLO intermediate (M_5Gn_2-P-P-Dol) is first synthesized by seven cytosolic glycosyltransferase reactions upon a Dol-phosphate (Dol-P) carrier lipid, using the nucleotide sugars UDP-GlcNAc and GDP-mannose. After transmembrane flipping, $G_3M_9Gn_2$-P-P-Dol is then formed by seven additional lumenal reactions using

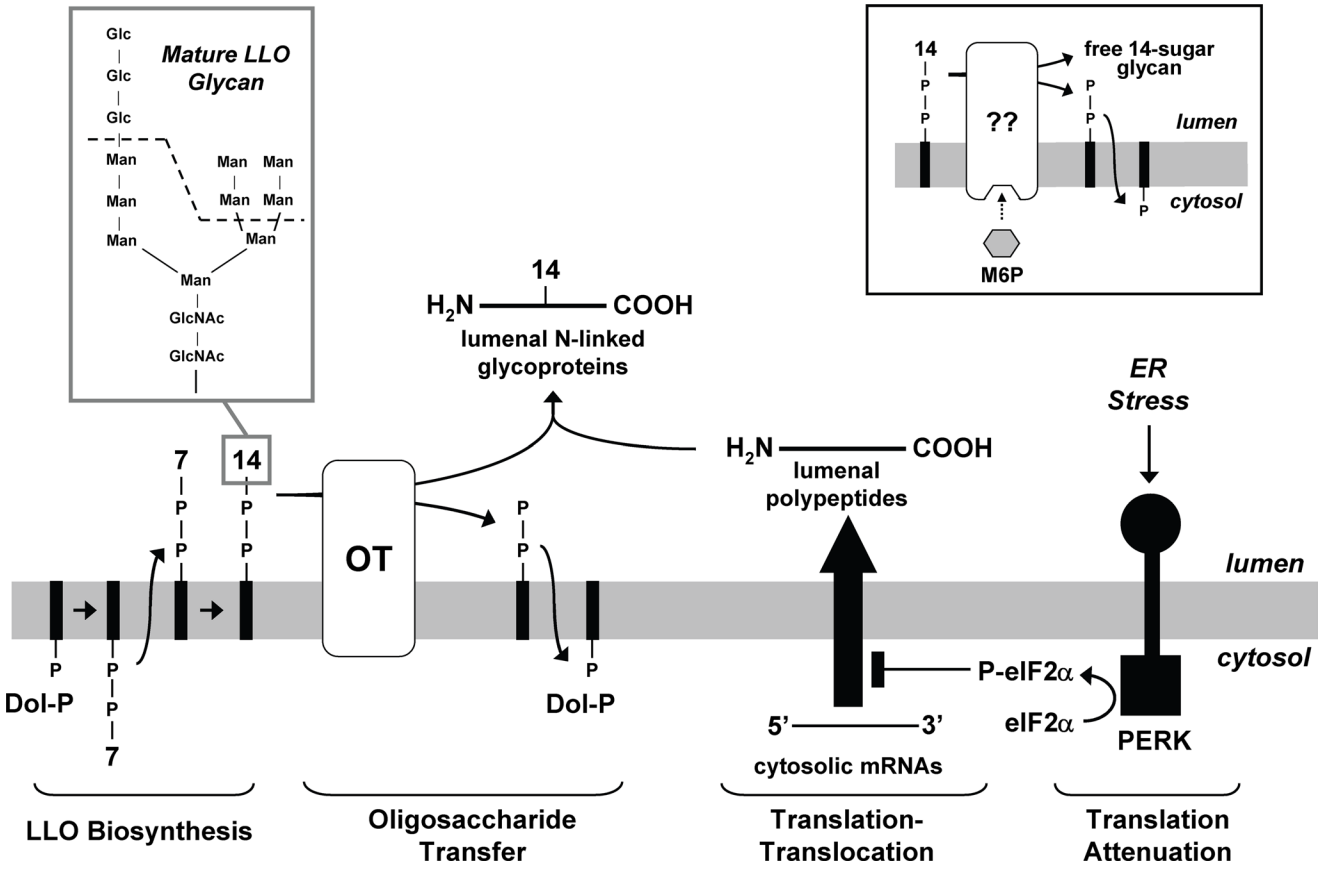

FIGURE 1: ER stress reduces LLO consumption due to *N*-glycosylation. In response to ER stress, PERK is activated to phosphorylate eIF2α, attenuating translation. This diminishes nascent polypeptide chains inside the ER lumen. As many of these polypeptides are acceptors for OT, this also lowers consumption of mature LLOs, functionally coupling LLO flux to glycoprotein synthesis (Shang *et al.*, 2007). Dol-P-P (facing the lumen) released during LLO consumption is recycled to Dol-P, which faces the cytosol (dolichols are indicated by black rectangles). Cytosolically oriented Dol-P serves as the carrier for assembly of a seven-sugar glycan intermediate coupled by a pyrophosphate linkage. After transmembrane flipping, extension to a 14-sugar glycan results in formation of mature LLO. The 14-sugar glycan is presented at the upper left, with the dashed line showing the seven-sugar intermediate. The inset at the upper right illustrates a reaction identified with permeabilized mammalian cells, in which cytosolic M6P causes cleavage of mature LLO and generation of a free 14-sugar glycan. Presumably, M6P activates a catalytic ER membrane component (Gao *et al.*, 2005).

mannose-P-Dol and glucose-P-Dol as donors, themselves generated with GDP-mannose and UDP-glucose (Kornfeld and Kornfeld, 1985; Schenk *et al.*, 2001). The precursors of nucleotide sugars are simple hexose phosphates. For example, mannose-6-phosphate (M6P) is converted by phosphomannomutase to mannose-1-P (M1P), which is then reacted with GTP to form GDP-mannose.

The congenital disorders of glycosylation (CDG) are recessive human genetic diseases diagnosed by underglycosylation of serum glycoproteins, and likely involve aberrant *N*-glycosylation in most tissues (Jaeken and Matthijs, 2001; Marquardt and Freeze, 2001). CDG patients generally present with developmental, neurological, and metabolic abnormalities during early childhood, often with poor survival. CDG type Ia, by far the most commonly diagnosed form of CDG, is caused by mutations affecting the *PMM2* gene encoding phosphomannomutase. The disease is thought to result from insufficient formation of M1P by this enzyme, with compromised production of GDP-mannose for LLOs and other mannosylated glycoconjugates. However, it is also possible that dysfunctional PMM2 results in accumulation of M6P, the enzyme's substrate, which is in some way detrimental to the LLO pool. This concept is supported by work using a defined system for LLO biosynthesis, where addition of 50 μM M6P caused specific degradation of $G_3M_9Gn_2$-P-P-Dol in a variety of streptolysin-O (SLO)-permeabilized mammalian cells (dermal fibroblasts, CHO-K1 cells, and primary hepatocytes), and release of free $G_3M_9Gn_2$ (Gao *et al.*, 2005; Figure 1, right, inset). In this system, LLO intermediates smaller than $G_3M_9Gn_2$-P-P-Dol were not sensitive to M6P-dependent cleavage, and structurally related M6P analogues, including glucose-6-P (G6P) and M1P were ineffective. These findings strongly suggest that M6P modulates a discrete target in the LLO pathway to cause $G_3M_9Gn_2$-P-P-Dol degradation.

Though highly specific in nature, the context and purpose of the M6P-dependent LLO cleavage detected in permeabilized cells remains unknown. We previously reported how one stress-signaling pathway can balance LLO flux with client polypeptide load (Shang *et al.*, 2007; Figure 1). In this paper, we report that M6P-dependent $G_3M_9Gn_2$-P-P-Dol degradation represents the terminus of a second, unique, stress-activated pathway in intact cells, in which M6P behaves as a signaling molecule for regulated LLO destruction. This result prompted us to reassess LLO fate in the context of viral infection, a well-known paradigm for *N*-glycosylation. In particular, we find that ER stress, M6P production, and LLO destruction are triggered by infection with the *N*-glycosylated pathogen herpes simplex virus 1 (HSV-1), suggesting a potential host-defense mechanism. We speculate that the etiology of CDG-Ia, in which M6P accumulation is predicted, may involve this mechanism having gone awry.

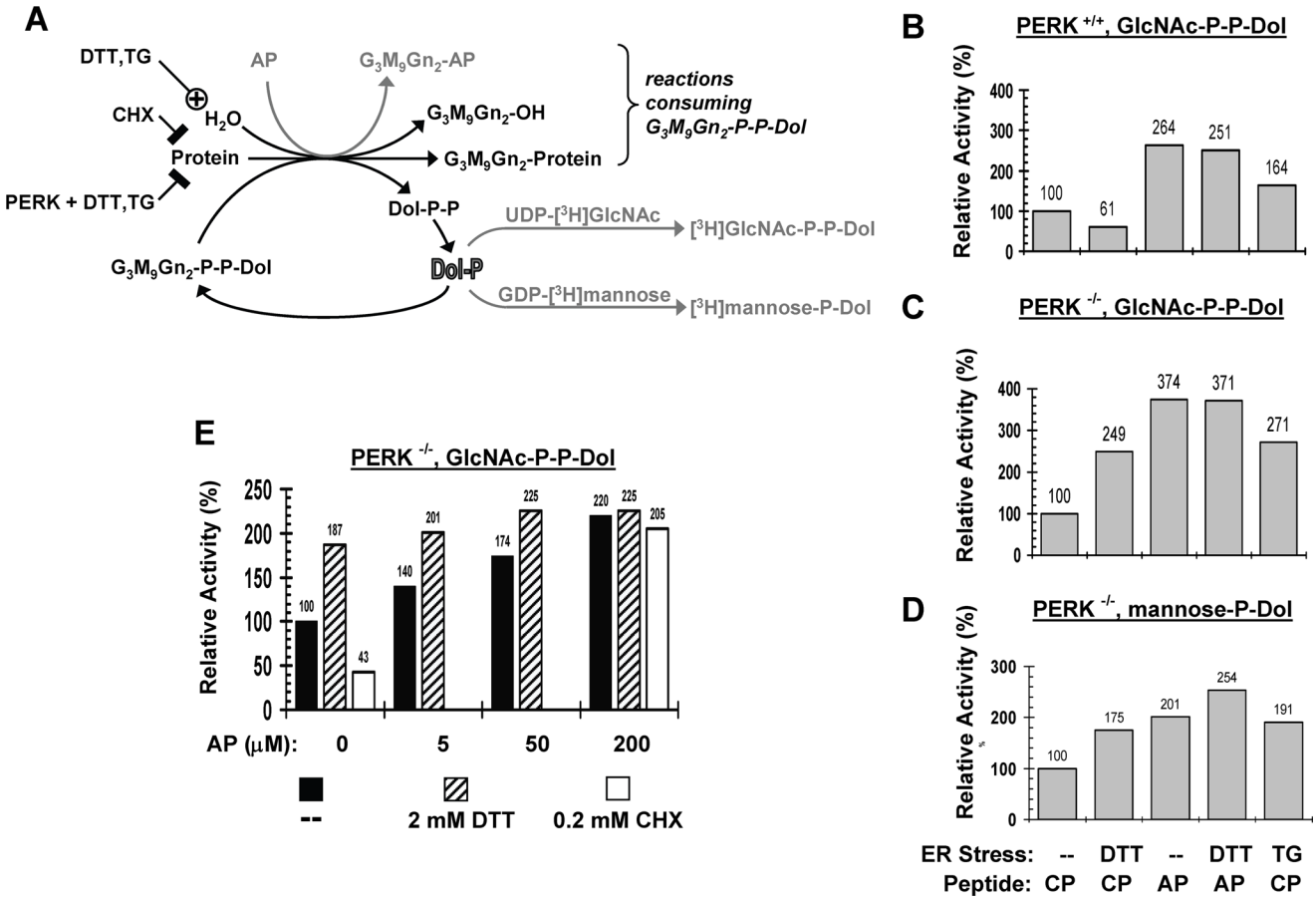

FIGURE 2: ER stress causes release of Dol-P from a preexisting LLO pool. (A) Influences of ER stressors and other factors on the dolichol cycle, and assay of Dol-P with nucleotide-[^{3}H]sugars. Reactions in black occur in intact cells, and those in gray are in SLO-permeabilized cells. $G_3M_9Gn_2$-P-P-Dol is consumed by transfer of glycan to protein, water (hydrolysis), or OT AP; Dol-P is regenerated in all cases. (B) PERK$^{+/+}$ and (C–E) PERK$^{-/-}$ MEFs were left untreated (–) or treated for 1 h with 2 mM DTT, 150 nM TG, or 200 μM CHX, as indicated. After permeabilization with SLO, they were incubated with either UDP-[^{3}H]GlcNAc (B, C, and E) or GDP-[^{3}H]mannose (D); this procedure assays the limited pool of Dol-P restricted to the dolichol cycle (Gao and Lehrman, 2002b). Some incubations contained 50 μM (B–D) or variable (E) concentrations of a control tripeptide (CP) unable to serve as OT substrate, or AP. Condition labels under (D) also apply to (B and C). [^{3}H]lipids were determined by liquid scintillation spectroscopy. Bars are labeled with percent activities and are the averages of duplicates. The highest ranges among duplicates were ± 5, 6, 19, and 10%, for (B–E), respectively.

RESULTS

Initial evidence for regulated LLO destruction in intact cells—generation of Dol-P by ER stress

Transfer of the 14-sugar $G_3M_9Gn_2$ glycan from LLO to nascent ER polypeptide yields Dol-P-P as a byproduct, which is efficiently recycled to Dol-P to seed a new round of LLO synthesis (Schenk *et al.*, 2001; Figure 1). As shown by others (Spiro *et al.*, 1976; Schmitt and Elbein, 1979; Hubbard and Robbins, 1980; Grant and Lennarz, 1983) and reproduced by us (Gao and Lehrman, 2002b), this "dolichol cycle" is interrupted by inhibitors of protein synthesis such as cycloheximide (CHX), which traps the Dol-P in LLO molecules. It therefore seemed reasonable that physiological stimuli that slow translation would also hinder the dolichol cycle and diminish Dol-P availability. One such translation-attenuating activity is mediated by the ER-associated transmembrane kinase "PKR-like ER kinase" (PERK, also known as PEK [Sood *et al.*, 2000]). PERK has a lumenal stress-sensing domain and a cytosolic Ser/Thr kinase domain. In response to ER stress, PERK phosphorylates the translation initiation factor eIF2α, which results in attenuated translation initiation for ER client polypeptides (Figure 1). Thus, we devised experiments to test the hypothesis that PERK activation would trap a large portion of the Dol-P pool as LLO.

Dol-P levels in normal mouse embryonic fibroblasts (MEFs) with functional PERK were consequently evaluated after treatment with either of two well-known ER stressors: dithiothreitol (DTT), which reduces disulfide bonds of ER proteins; and thapsigargin (TG), which blocks ER calcium channel ATPase activity, resulting in calcium loss. As for the M6P-dependent reaction discussed in the *Introduction*, proper measurement of Dol-P in the dolichol cycle requires retention of fragile ER structure by gentle permeabilization with SLO. This procedure is unlike those employing homogenization and isolation of microsomal membranes, which obscure this pool of Dol-P (Gao and Lehrman, 2002b). Thus, SLO treatment permits reliable study of the dolichol cycle with radioactive nucleotide sugar donors for Dol-P-dependent enzymes. Figure 2A presents the reactions and reagents used in this analysis.

In the first step of LLO formation, UDP-GlcNAc donates GlcNAc-1-P for Dol-P-dependent synthesis of GlcNAc-P-P-Dol (Lehrman, 1991). Treatment with a three–amino acid OT acceptor peptide (AP), resulting in transfer of the LLO-associated glycan to the peptide and generation of Dol-P, increased GlcNAc-P-P-Dol synthesis in PERK$^{+/+}$ samples to ~260% of control levels (Figure 2B). Although PERK-dependent translation attenuation was expected to strongly

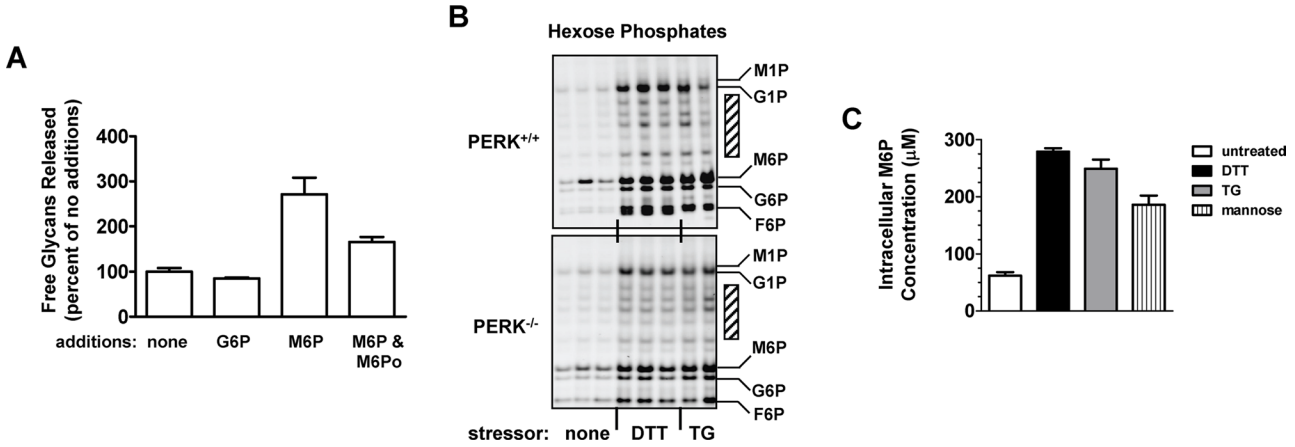

FIGURE 3: ER stress elevates M6P. (A) SLO-permeabilized normal ($MPI^{+/+}$) MEFs were incubated 1 h at 37°C with nucleotide sugar LLO precursors in the absence or presence of 100 μM G6P, 100 μM M6P, and/or 200 μM M6Po. Released free glycans (G_4–G_7 equivalent pool) measured by FACE are expressed as percent of untreated controls (duplicates ± range). (B) FACE gels showing hexose-Ps of $PERK^{+/+}$ and $PERK^{-/-}$ MEFs, either unstressed (triplicates) or stressed (2 mM DTT [triplicates] or 150 nM TG [duplicates]) for 1 h. Cells were ~80% confluent. Electrophoresis is top to bottom. Positions of AMAC-conjugated standards are labeled. When required, G1P-AMAC and M1P-AMAC were resolved by running gels longer (e.g., see Figure 6B, upper). Although labeled as hexose-1-Ps for clarity, FACE analysis requires dephosphorylation of M1P and G1P prior to AMAC conjugation. Cross-hatched bars indicate unidentified AMAC conjugates increased by ER stress. (C) Intracellular M6P concentrations (μM) in $PERK^{-/-}$ MEFs (averages of duplicates ± range) after no treatment (white) or treatments with DTT (2 mM, 1 h, black), TG (150 nM, 1 h, gray), or D-mannose (10 mM, 1 h, vertical stripes).

decrease GlcNAc-P-P-Dol synthesis by depleting Dol-P, only a mild loss of GlcNAc-P-P-Dol was measured with DTT (~60% of control levels). More surprisingly, an increase (~160% of control levels) in activity was detected with TG. Together, these data suggested that two opposing effects were in play: the anticipated suppression of Dol-P levels by ER stress due to PERK-dependent translation attenuation (Figure 1), and offsetting production of Dol-P by an unknown effect of ER stress. Testing this hypothesis with $PERK^{-/-}$ MEFs (Figure 2C) revealed that treatments with DTT or TG each substantially increased Dol-P (~250% of unstressed controls). This represented a large fraction of the Dol-P in $PERK^{-/-}$ MEFs that could be released from LLO by discharge with AP (~370% of controls). When mixed, the effects of DTT and AP were not additive, suggesting they acted upon the same pools of LLO and Dol-P (Figure 2, C–D), and DTT was not behaving as a nonspecific enzyme stimulator.

These results with $PERK^{-/-}$ MEFs were not limited to the GlcNAc-1-P transferase itself, because similar effects were detected with GDP-mannose used to evaluate Dol-P-dependent mannose-P-dolichol synthesis (product was increased to ~180% of unstressed controls by ER stress [Figure 2D]). In sharp contrast to ER stressors, CHX reduced GlcNAc-P-P-Dol synthesis to ~45% of unstressed controls, demonstrating that the dolichol cycle had the expected sensitivity to translation rate (Figure 2E). The ability of CHX to trap Dol-P as LLO was countered by acceptor peptide, which released the trapped Dol-P. As in Figure 2C, the effects of the DTT and AP treatments shown in Figure 2E were not additive.

Since DTT could not supplement the effects of AP, ER stress did not appear to cause new Dol-P synthesis. Rather, the results were best explained by ER stress liberating Dol-P from preformed LLO, as did AP, by cleavage within the pyrophosphate linkage (accompanied if necessary by either pyrophosphatase or dolichol kinase action [Schenk *et al.*, 2001]). As shown in Figure 2B, active PERK obscured this observation. Consequently, for clarity, most of our subsequent biochemical analysis of this unexpected LLO degradation was performed with $PERK^{-/-}$ MEFs, although key results were repeated with $PERK^{+/+}$ MEFs.

ER stress increases M6P and decreases steady-state LLO levels

No signaling pathways are known that explain LLO cleavage and Dol-P generation in ER-stressed MEFs indicated in the schematic in Figure 2. As reviewed in the *Introduction*, we previously demonstrated that M6P can stimulate release of free glycans from LLO in permeabilized cells (Figure 1, inset), and therefore speculated this mechanism might be utilized by cells under the type of ER stress induced by DTT and TG. This hypothesis makes several testable predictions: 1) ER stress should elevate M6P to concentrations sufficient to induce LLO cleavage; 2) elevated M6P levels caused by ER stress should decrease LLOs and increase the products of their cleavage—namely Dol-P (Figure 2) and free glycans; and 3) the process should be regulated by an authentic ER stress–sensing molecule. We thus set about testing these predictions systematically, beginning with an assessment of M6P responsiveness and levels in MEFs.

We used fluorophore-assisted carbohydrate electrophoresis (FACE) as a general method for profiling steady-state levels of intracellular saccharides and associated molecules (e.g., LLOs). FACE takes advantage of fluorophore conjugation to carbohydrates, with differing purification schemes and fluorophore reactivities useful in profiling different carbohydrate species. FACE also has the advantage of not requiring glucose deprivation of cells, which is often used during metabolic labeling studies and which is capable of perturbing ER function and saccharide analysis (Gao and Lehrman, 2002a; Lehrman, 2007). Using FACE, we first asked whether M6P specifically stimulated release of $G_3M_9Gn_2$ in SLO-treated MEFs, a permeabilized cell type that had not been previously evaluated for this reaction.

As shown in Figure 3A, 50 μM M6P, but not G6P, promoted $G_3M_9Gn_2$ release from LLO in SLO-permeabilized MEFs, indicating these cells contained the components needed to respond to M6P. We previously reported that several hexose-Ps in mammalian cells were mobilized by ER stress, presumably to aid glycoconjugate synthesis and ATP production (Doerrler and Lehrman, 1999;

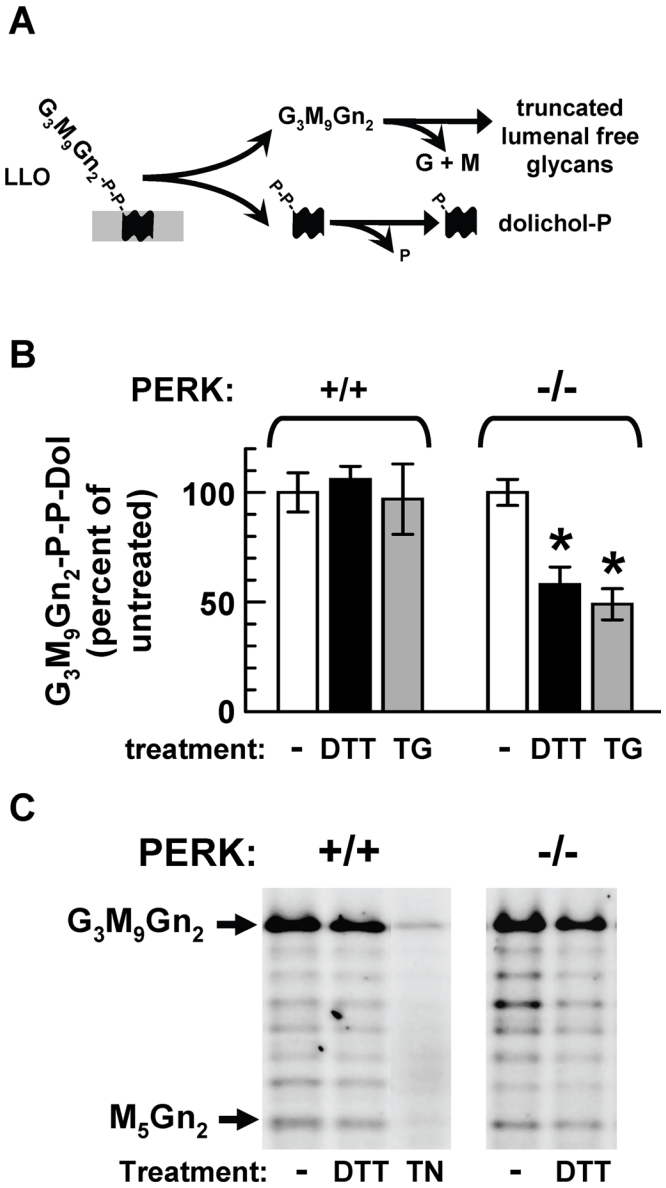

FIGURE 4: LLO destruction in ER-stressed MEFs. (A) LLO cleavage is expected to elevate levels of Dol-P/Dol-P-P and lumenal free glycans, the latter digested by lumenal glycosidases. (B) FACE measurements of $G_3M_9Gn_2$-P-P-Dol for DTT- (black) or TG- (gray) treated PERK$^{+/+}$ and PERK$^{-/-}$ MEFs, expressed as percentages for untreated (white) cells (mean ± SEM; n = 4 and 6, respectively; ∗, $p < 0.0001$ compared with unstressed control). (C) FACE gels of LLOs from PERK$^{+/+}$ and PERK$^{-/-}$ MEFs after treatment with DTT or TN (5 μg/ml, 1 h) show that ER stress does not degrade the glycan component. Standards are indicated.

Gill *et al.*, 2002). To determine specifically whether M6P increased in ER-stressed MEFs, we coupled cellular pools of hexose-Ps to the FACE fluorophore 2-aminoacridone (AMAC). As shown in Figure 3B, glucose-1-P (G1P), G6P, fructose-6-P (F6P), and M6P (as well as several unidentified species) were all increased by DTT and TG. When corrected for cellular volume, M6P concentrations in PERK$^{-/-}$ MEFs increased about fourfold, from 60 μM to 250 μM (Figure 3C). Notably, G1P is a direct product and the other hexose-Ps are indirect products of glycogen breakdown by glycogen phosphorylase (GP).

These data showed that MEFs contain the M6P-responsive component(s) needed for LLO cleavage, and that ER stress can increase M6P in intact MEFs in the required concentration range. To directly assess whether the elevated M6P might have caused LLO cleavage, and therefore provide an explanation for the generation of Dol-P (Figures 2 and 4A) in intact stressed MEFs, we used a variation of the FACE technique in which the glycan portions of LLOs were released from the lipid carrier with mild acid, and then labeled with the fluorophore 7-amino-1,3-naphthalenedisulfonic acid (ANDS; Gao and Lehrman, 2006; Lehrman, 2007). Interestingly, both DTT and TG stresses resulted in a statistically significant suppression of $G_3M_9Gn_2$-P-P-Dol levels in PERK$^{-/-}$ MEFs (Figure 4B). No truncated LLOs were generated (Figure 4C). Thus, there was no degradation within the LLO glycan moiety, further supporting the hypothesis that ER stress activated LLO cleavage within the pyrophosphate linkage.

ER stress causes the appearance of LLO-derived free glycans

Using FACE, we next measured levels of free glycans predicted by hydrolysis of $G_3M_9Gn_2$-P-P-Dol (Figure 4A). Conjugation of the ANDS fluorophore requires a reducing end on the oligosaccharide, which could result from cleavage between the reducing terminal GlcNAc and the pyrophosphate linkage, or cleavage within the pyrophosphate linkage followed by dephosphorylation of the resulting phospho-oligosaccharide. After DTT or TG treatments, free glycan pools in PERK$^{-/-}$ MEFs were altered significantly (Figure 5A) with an approximately twofold increase of the total pool (presented below in Figure 6). Although $G_3M_9Gn_2$ itself was not apparent in free glycan pools, it could be preserved by inclusion of the glucosidase inhibitor castanospermine (Figure S1), consistent with rapid digestion by intracellular glycosidases. However, castanospermine was not used routinely in our experiments because it causes ER stress (Doerrler and Lehrman, 1999).

Significantly, free glycans released by ER stress were sensitive to diagnostic enzymatic digestions for LLO-type structures. Glycans that migrated more slowly than the G_6 standard (Figure 5B), in the range expected for M_6Gn_2 to $G_3M_9Gn_2$, were susceptible to endoglycosidase H—an enzyme that senses the presence of a specific α1,3-linked mannosyl residue on mature LLOs and many of the larger LLO intermediates. Moreover, all of the glycans were sensitive to jack bean α-mannosidase. This enzyme cleaves exposed α-linked mannosyl residues expected on LLO-derived glycans. The observation of a resistant fragment in the G_5–G_6 range is consistent with the presence of blocking glucosyl residues, which are also a feature of some LLO-derived glycans. Tunicamycin (TN), an inhibitor of LLO synthesis as well as an inducer of ER stress, did not increase free glycans (Figure 5A).

These data were highly consistent with destruction of LLO by ER stress, yielding Dol-P and free glycans (Figure 4A). However, a possibility remained that the free glycan increases were actually caused by ERAD of nascent glycoproteins destabilized by ER stressors (Figure 5C). This could be especially severe in PERK$^{-/-}$ MEFs, which are unable to limit new glycoprotein synthesis in response to ER stress. To distinguish between LLO cleavage and ERAD, we analyzed the subcellular compartmentalization of the free glycans. Glycans increased by ERAD should be cytosolic, while LLO-derived glycans should be lumenal (Chantret and Moore, 2008). These populations can be distinguished as retained (lumenal) and diffusible (cytosolic) glycan pools after permeabilization with SLO (Moore *et al.*, 1995; Figure 5C).

As expected, the two types of free glycan pools in MEFs were distinctly different (Figure 5D). Significantly, both DTT and TG increased lumenal free glycan pools, while there were no effects on

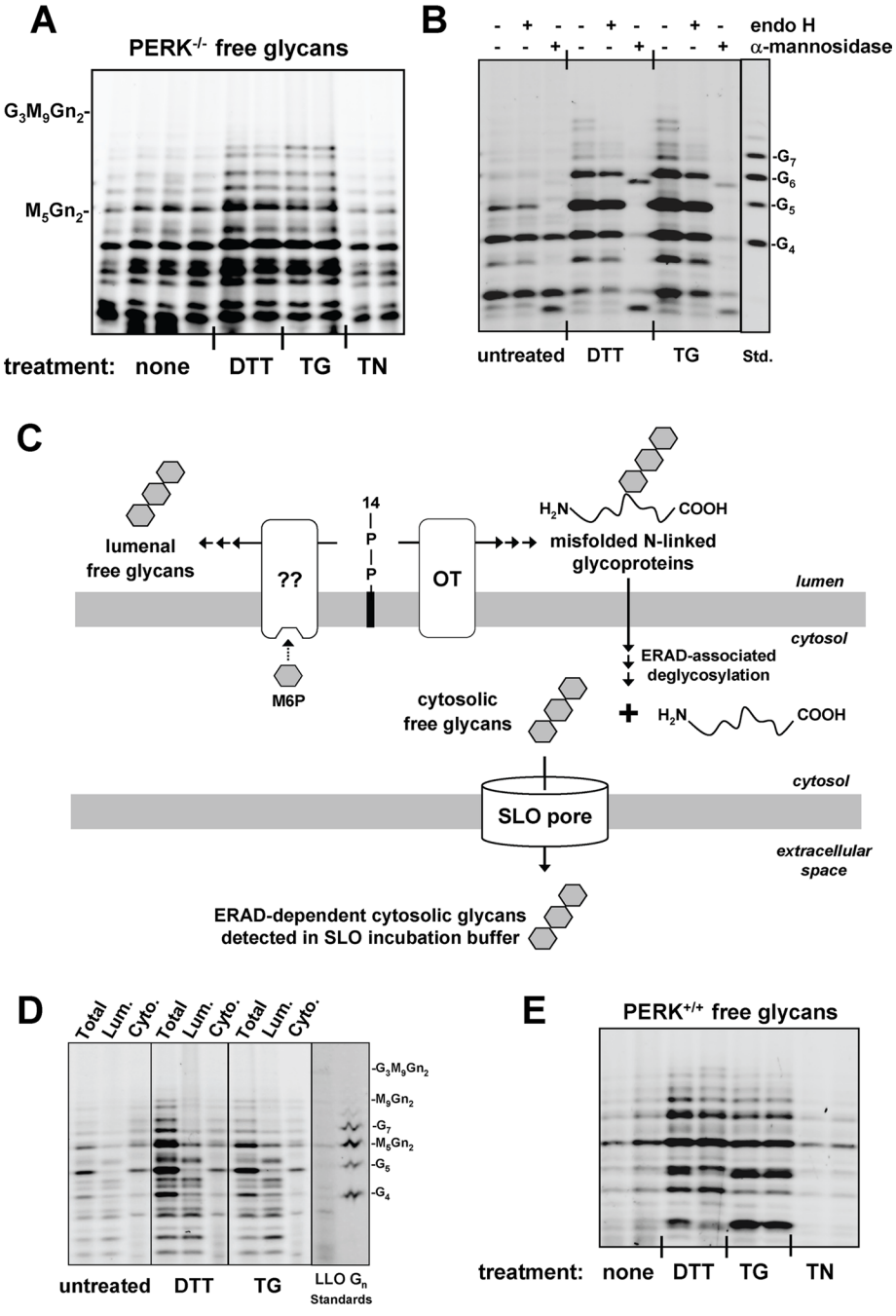

FIGURE 5: ER stress generates LLO-derived lumenal free glycans. (A) Free glycans in PERK$^{-/-}$ MEFs after treatments with DTT, TG, or TN. The positions of M_5Gn_2 and $G_3M_9Gn_2$ standards on FACE gels are shown. (B) PERK$^{-/-}$ MEFs were left untreated, or treated 1 h with either 2 mM DTT or 150 nM TG. ANDS-conjugated free glycans were incubated in the absence or presence of endoglycosidase H or α-mannosidase. Note that Gn_1-ANDS generated by endoglycosidase H runs off the gel. (C) Free glycans released from LLOs in response to M6P are predicted to be in the ER lumen. In contrast, free glycans from protein misfolding, export from the lumen, and enzymatic deglycosylation during ERAD should be cytosolic. In both pathways, glycans can be digested by various exoglycosidases (indicated by the repeating arrows) to generate heterogeneous structures. The lumenal and cytosolic glycan pools can be distinguished by SLO permeabilization. See Figure 1 for explanation of symbols. (D) After treatment of PERK$^{-/-}$ MEFs with DTT or TG, free glycans were analyzed directly from whole cells (Total), or after permeabilization with SLO, to yield lumenal free glycans (Lum.) in cell bodies and cytosolic free glycans (Cyto.) in permeabilization medium. In this and similar experiments, we noticed that the Total signals appear greater than the sums of the lumenal plus cytosolic signals, presumably due to sample loss occurring during the additional SLO step. (E) PERK$^{+/+}$ MEFs, as for (A).

cytosolic pools. This showed that ER stress caused LLO cleavage, but without a free glycan contribution by ERAD. Further, z-VAK-fmk (an inhibitor of cytosolic *N*-glycanase [Misaghi *et al.*, 2004]), did not prevent the ER stress–dependent increase of free glycans. Experiments presented in the next section with inhibitors of glycogen phosphorylase also address ERAD.

In summary, ER stress–induced increases of M6P in intact cells correspond with loss of $G_3M_9Gn_2$-P-P-Dol and appearance of LLO-derived Dol-P and lumenal free glycans. While fastidious LLO biosynthesis is critical for proper *N*-linked glycosylation, our results suggested M6P might have a paradoxical function in impeding LLO usage. The experiments that follow, which were intended to further elucidate M6P's role, evaluated the metabolic origin of M6P, its necessity for LLO cleavage, and its signaling pathway.

ER stress–dependent M6P originates from glycogen and is necessary for LLO cleavage

We considered hypotheses for both intracellular and extracellular sources of the ER stress–generated hexose-Ps. Since ER stress does not appear to stimulate hexose transport or hexokinase activities (Doerrler and Lehrman, 1999; Gill *et al.*, 2002), it was unlikely that intracellular hexose-Ps were increased by these mechanisms. In contrast, ER stress did correlate with decreased glycogen content (Gill *et al.*, 2002), and it also correlated with increases in metabolites of glycogenolysis (Figures 3B and 6A), suggesting that glycogen may be an intracellular source of these sugars.

The hypothesis that ER stress triggered glycogenolysis was tested by treating ER-stressed MEFs with a highly efficacious inhibitor of GP, the indole-2-carboxamide CP-91149 (Figure 6A; Martin *et al.*, 1998). As shown in Figure 6B, CP-91149 efficiently blocked the appearance of all DTT- and TG-inducible G1P, the immediate product of glycogenolysis. Equally as important, blocking glycogenolysis with CP-91149 also prevented the increases of G6P, F6P, and M6P (Figure 6C), all of which can be formed from G1P (Figure 6A). To address the possibility that a nonglycogen source of sugars was blocked by an unexpected off-target activity of CP-91149, we evaluated two additional GP inhibitors having different mechanisms than CP91149. While CP-91149 interacts with a novel GP site (Oikonomakos *et al.*, 2000; Rath *et al.*, 2000), caffeine inhibits the known purine-binding site (Johnson, 1992), and

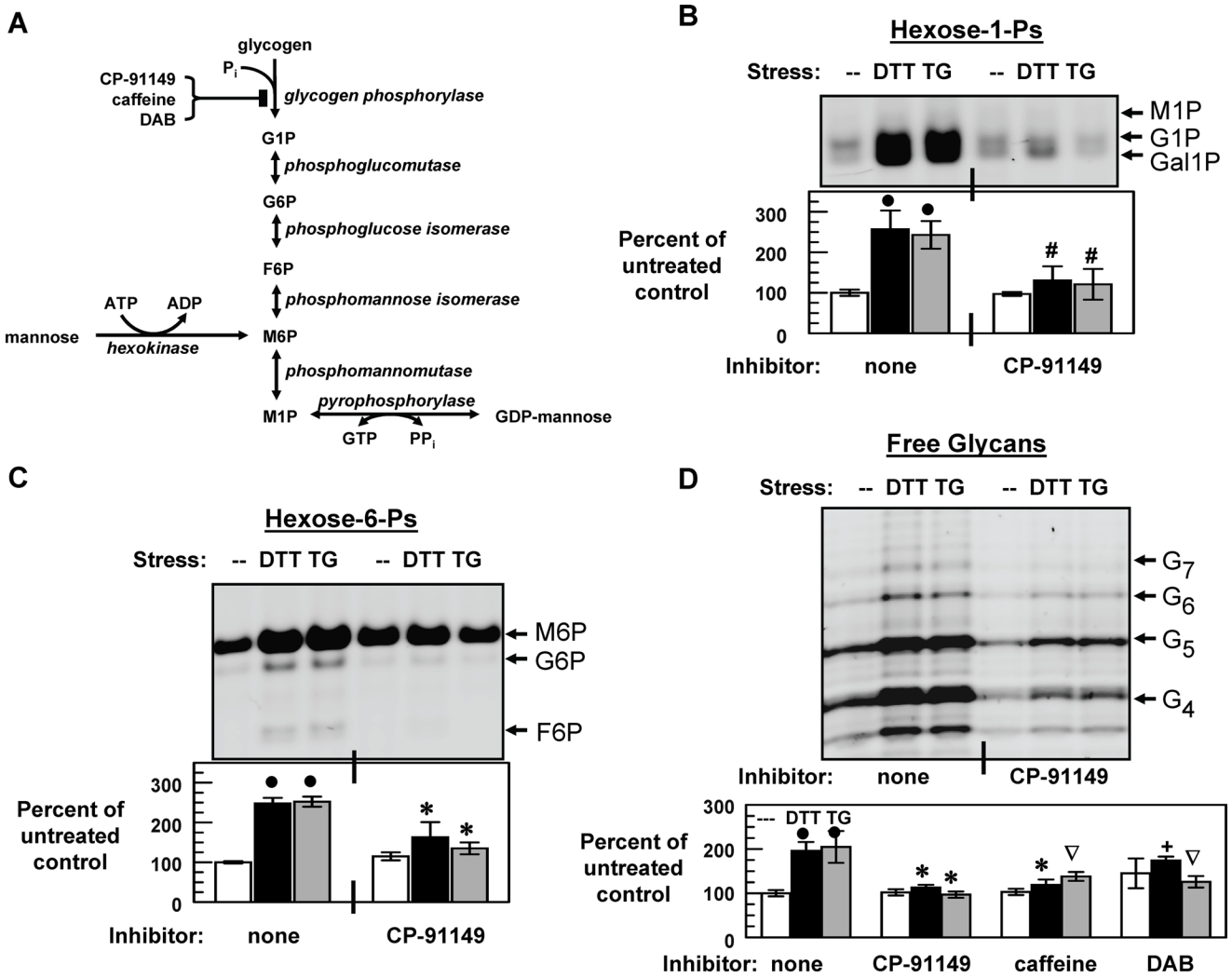

FIGURE 6: Glycogen phosphorylase inhibitors block ER stress–induced hexose-P mobilization and free glycan increases. (A) Scheme linking glycogenolysis and extracellular mannose to hexose-Ps and GDP-mannose. Three GP inhibitors are indicated. Determinations of (B) hexose-1-Ps, (C) hexose-6-Ps, and (D) free glycans. Where indicated, PERK$^{-/-}$ MEFs were either left unstressed (white bars) or stressed with 2 mM DTT (black) or 150 nM TG (gray) for 1 h prior to saccharide harvest, in the absence or presence of 50–100 μM CP-91149, 5 mM caffeine, or 20 μM DAB (each for 2 h prior to saccharide harvest). Each panel includes one representative FACE gel (upper) and averaged data from four independent FACE experiments (lower), measuring total pools of hexose-Ps or the G_4–G_7 equivalent pool of free glycans. •, $p < 0.001$ for all inhibitor-free stressed samples compared with inhibitor-free unstressed controls. ⁎, $p < 0.001$; #, $p < 0.005$; ∇, $p < 0.01$; +, $p < 0.08$ for inhibitor-treated stressed samples compared with inhibitor-free stressed samples.

1,4-dideoxy-1,4-imino-D-arabinitol (DAB) targets the catalytic site (Oikonomakos *et al.*, 2006). Like CP-91149, these two GP inhibitors impaired DTT- and TG-dependent hexose-P mobilization (unpublished data). From these experiments and earlier results (Gill *et al.*, 2002), we conclude that glycogen is the source of ER stress–dependent hexose-Ps.

If LLO cleavage is caused by M6P produced via ER stress–dependent glycogenolysis, then GP inhibitors should prevent the formation of LLO-derived free glycans. As shown in Figure 6D, this was indeed the case: CP-91149, caffeine, and DAB each hindered DTT- and TG-dependent free glycan increases. These results also further ruled out a contribution by ERAD (which should have been insensitive to these inhibitors), as well as LLO cleavage by a nonspecific effect of ER stress on the labile pyrophosphate bond. Collectively, these results link ER stress to glycogenolysis, elevated M6P, and LLO cleavage.

M6P introduced in the absence of ER stress is sufficient to cause LLO cleavage

To test the sufficiency of M6P for LLO cleavage by an independent method, we introduced it into cells at appropriate concentrations, but in the absence of ER stress. As shown in Figures 7, A–C, a 60-min incubation of PERK$^{-/-}$ MEFs in medium supplemented with 10 mM D-mannose increased intracellular M6P by three- to sixfold, to ~180 μM (Figure 3C). Using analyses similar to those described in the preceding sections for ER-stressed cells, we found that these conditions stimulated LLO cleavage: $G_3M_9Gn_2$-P-P-Dol decreased to 82 ± 2% (n = 2) of untreated levels, and significantly, lumenal free glycans increased (Figures 7, A–D). There was no effect of incubation with 10 mM D-galactose, the 2- and 4-epimer of D-mannose. LLO cleavage was therefore not explained by nonspecific osmotic factors.

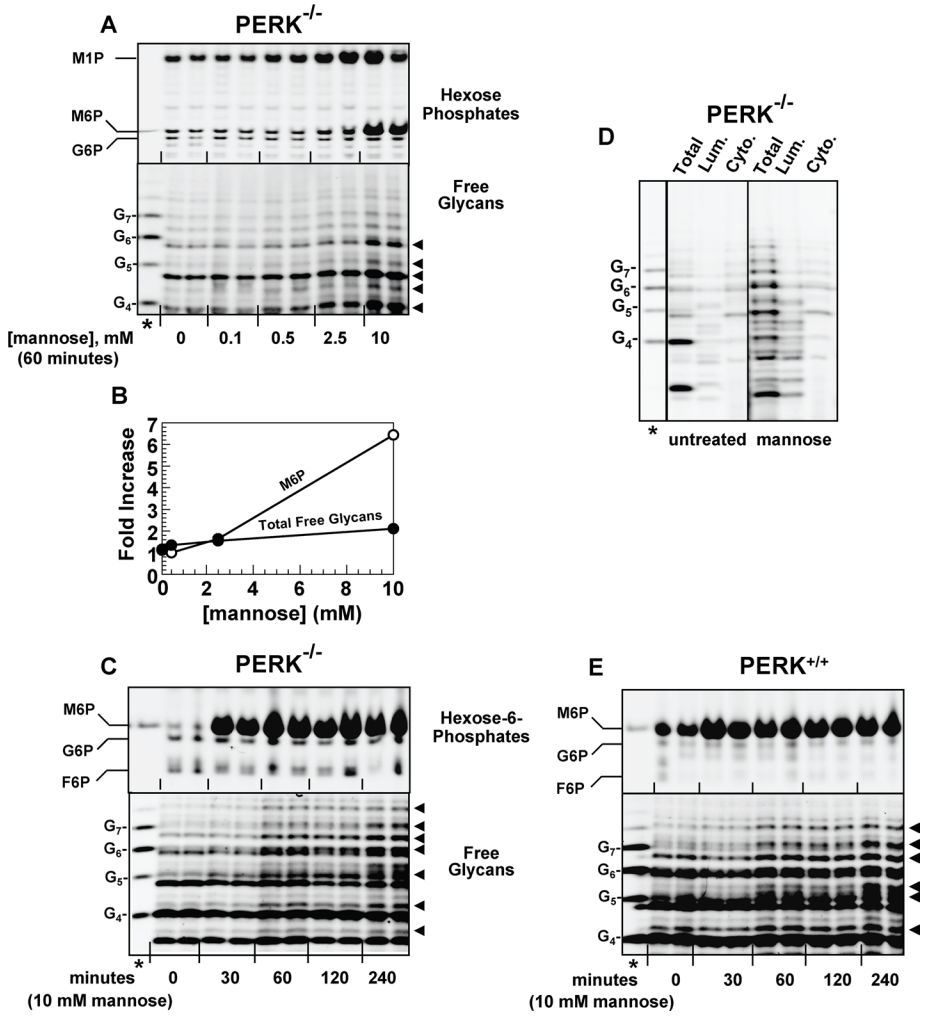

FIGURE 7: Elevation of M6P in the absence of ER stress releases free glycans. (A–D) PERK$^{-/-}$ MEFs were incubated with (A, B) variable concentrations of mannose for 60 min; (C) 10 mM mannose for variable times; or (D) 10 mM mannose for 60 min. (A and C) Hexose-Ps (top) and free glycans (bottom) as in Figures 3B, 5A, and 6B. Black arrowheads indicate glycans increased by mannose treatment. (B) Quantitative measurements (averages of duplicates) of M6P (white) and total free glycans migrating in the G_4–G_7 standard range (black) from (A). (D) Lumenal and cytosolic free glycans from untreated or mannose-treated cells were separated, as in Figure 5D. Standard lanes are marked with asterisks. (E) As for (C), with PERK$^{+/+}$ MEFs.

Mannose treatment itself did not cause ER stress, because stress-associated hexose-6-Ps other than M6P (i.e., G6P and F6P) were not elevated (Figure 7, A and C). Mannose treatment of MEFs did not increase GRP78/BiP mRNA, and neither brief nor extended mannose treatments increased splicing of XBP1 mRNA (Figure S2), both sensitive markers for ER stress signaling. Mannose treatment generated free glycans even during CHX treatment, to prevent synthesis of newly synthesized glycoproteins, which might be ERAD substrates and hence glycan sources (unpublished data). Therefore, we find no evidence that the free glycans generated by mannose treatment were due to inadvertent ER stress or ERAD.

As seen in Figure 7A, 10 mM mannose treatment increased both M6P and M1P. However, M1P was not increased by ER stress, and none of the other ER stress-induced metabolites of glycogenolysis (G1P, G6P, and F6P) were increased by mannose treatment. Thus M6P was the only hexose-P increased under all conditions causing LLO cleavage. It is unclear why elevated M6P appeared to drive formation of M1P (a single enzymatic step; Figure 6A) after mannose incubation; but not with ER stress; perhaps ER stress also promotes reactions that consume M1P. Coupled with the strong specificity for M6P in permeabilized cell experiments (Figure 3A; Gao *et al.*, 2005), we conclude that increased M6P is sufficient to drive LLO cleavage in intact cells, even in the absence of ER stress.

Inhibition by a structural analogue reveals a defined M6P target

Taken together, our data surprisingly implicate M6P as a signaling molecule. As such, it would be predicted to have a defined target, and be regulated by other signaling components. To understand these biological properties in greater detail, we adopted two approaches. First, we probed for the presence of an M6P interaction site in LLO cleavage reactions. Second, we sought to identify the signal transducer that triggers glycogenolysis (and hence M6P production) in response to ER stress. Some aspects of the M6P interaction site could already be deduced by our earlier permeabilized-cell experiments. Our findings that both M1P and G6P (the 2-epimer of M6P) failed to promote LLO cleavage suggested that the orientation of the 2-hydroxyl and the position of the phosphate in M6P are important for the M6P interaction and M6P-dependent signaling.

To further explore the requirements for M6P's interaction with a target site, we synthesized the nonhydrolyzable analogue mannose-6-phosphonate (M6Po; Figure S3A; compound 11 in Belakhov *et al.* [2004]). The M6Po preparation was free of detectable contaminating M6P (Figure S3B), and M6Po alone did not cause LLO cleavage with SLO-permeabilized cells (Figure S3C). However, inclusion of M6Po partially inhibited LLO cleavage caused by M6P, while inclusion of G6P or M1P had no effect (Figures 3A and S3D). The esterifying oxygen atom of M6P is therefore important for LLO cleavage, but not for binding to the M6P target site, allowing M6Po to antagonize M6P. It remains to be determined whether the esterifying oxygen mediates an activation step at the target site, and/or is involved in a requirement for M6P hydrolysis.

Authentic UPR signaling mobilizes hexose phosphates

To identify signaling components that might regulate M6P, we focused upon the abilities of DTT and TG to promote glycogenolysis, and considered two possibilities. First, as known ER stressors, DTT and TG might have triggered the unfolded protein response (UPR), an elaborate set of signaling events that occur in response to the presence of excess misfolded protein in the ER lumen (Schröder and Kaufman, 2005; Ron and Walter, 2007; Figure 8A). Alternatively, these agents may have unexpectedly altered hexose metabolic pathways by their effects on redox potential and calcium homeostasis. If the UPR was involved, hexose-P mobilization should be diminished by stable overexpression of GRP78/BiP

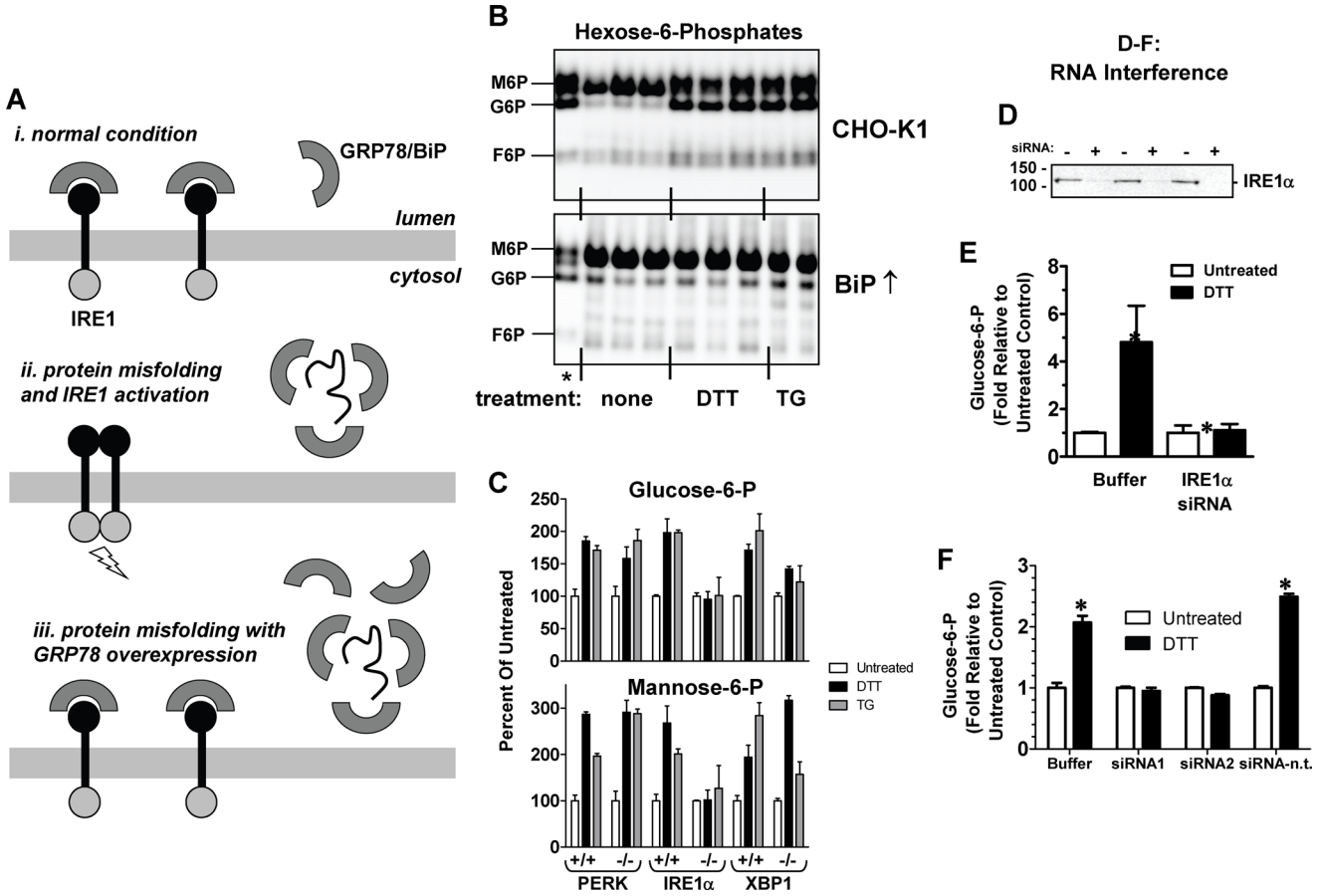

FIGURE 8: UPR signaling by IRE1α mobilizes hexose-Ps. (A) UPR-dependent actions of chemicals that cause protein misfolding can be distinguished from other possible effects of these chemicals by overexpression of GRP78/BiP. Under normal conditions, sufficient GRP78/BiP is available to complex with the lumenal stress-sensing domains of UPR signal transducers such as IRE1, maintaining them in an inactive state (i). In the presence of excess misfolded protein, GRP78 is no longer available to complex with IRE1, resulting in its dimerization and activation (ii). However, when GRP78 is overexpressed, there is sufficient GRP78 to suppress IRE1 signaling, even in the presence of excess misfolded protein (iii). (B) Hexose-Ps in untransfected (top) and GRP78/BiP-overexpressing (bottom) CHO-K1 cells after DTT or TG treatments. Asterisk denotes standard lane. While the effect on G6P is robust, changes in F6P and M6P are likely muted due to the enhanced glycolysis expected for these cells. (C) G6P (top) and M6P (bottom) levels in ER-stressed PERK$^{-/-}$, IRE1α$^{-/-}$, and XBP1$^{-/-}$ knockout MEFs as percentages of untreated cells, paired with genetically unmodified ($^{+/+}$) controls. For direct comparison, all cells were processed in a single experiment (also yielding Figure S4B), average of duplicates ± range. (D) Immunoblots (anti-IRE1α antibody) showing knockdown of IRE1α in normal (MPI$^{+/+}$) MEFs after RNA interference with a pool of four anti-IRE1α siRNAs. Protein size markers are shown. The three siRNA treatments used to generate the averaged data in (E) are shown. (E) G6P was measured by FACE after IRE1α knockdown in ER-stressed normal MEFs, expressed as fold change compared with buffer (no siRNA) controls, averaging three sets of duplicate determinations (n = 6, mean ± SEM; ∗, $p < 0.0002$ for untreated buffer controls compared with DTT-treated buffer samples, and for the latter compared with DTT-treated siRNA samples). (F) Relative G6P levels in untreated and DTT-stressed normal MEFs after RNA interference treatment as described in (E), with buffer only, siRNA1 alone, siRNA2 alone, or a pool of four nontargeting siRNAs (mean ± SEM, n = 3; ∗, $p < 0.0001$ for untreated buffer and nontargeting siRNA samples vs. corresponding DTT-treated buffer and nontargeting siRNA samples).

(Dorner *et al.*, 1992) to counteract dissociation of this chaperone from lumenal stress-sensing domains of UPR-signaling proteins and attenuate their activities (Figure 8A).

As shown in Figure S4A, overexpression of GRP78/BiP caused the expected reduction of UPR-dependent XBP1 splicing by either DTT or TG. Since the GRP78/BiP overexpressing cells were derived from tumor-like CHO-K1 cells, they were expected to have enhanced glycolysis (Levine and Puzio-Kuter, 2010), which could complicate hexose-P analysis; most of the F6P from glycogenolysis would likely be catabolized for ATP production, leaving little for conversion to M6P. We therefore focused on G6P, the intermediate preceding F6P, as an alternative readout for glycogenolysis (Figure 6A). As shown in Figure 8B, DTT and TG clearly elevated G6P in unmodified CHO-K1 cells, while G6P production was suppressed by overexpressing GRP78/BiP. Thus, one or more UPR-signaling proteins were responsible for mobilization of hexose-Ps.

Hexose-6-P mobilization is fast (detectable within 10 min of DTT application [Gill *et al.*, 2002]), arguing against transcriptional control. This focused our attention on the UPR transmembrane kinases PERK and inositol-requiring enzyme 1 (IRE1), which employ rapid autophosphorylation mechanisms and can be evaluated directly with MEF knockout lines. Knockout of PERK did not affect the abilities of

DTT or TG to mobilize G6P or M6P (Figures 3B and 8C). However, the response was blocked by knockout of IRE1α (Figure 8C). Three nucleotide sugars (UDP-GlcNAc, GDP-mannose, and UDP-glucose) synthesized from hexose-Ps also increased with ER stress, but also required IRE1α (Figure S4B). These results implicated IRE1α as an essential UPR component involved in glycogenolysis and hexose-P generation.

To independently assess the requirement for IRE1α, we used RNA interference. Suppression of IRE1α in normal MEFs with four pooled small interfering RNAs (siRNAs) caused 68–95% loss of IRE1α protein (Figure 8D) and inhibited hexose-P mobilization (Figure 8E). This result was extended with two individual siRNAs from the pool found most responsible for IRE1α suppression. Knockdown with either siRNA (designated siRNA1 and siRNA2, which reduced IRE1α protein to 48% or 38% of the buffer control, respectively) also prevented hexose-P mobilization. By comparison, a pool of four nontargeting siRNAs had no effect (Figure 8F). Taken together, knockout and knockdown experiments showed that IRE1α is necessary for hexose-P mobilization by the UPR.

Signaling by the IRE1α kinase domain triggers glycogenolysis

IRE1α is a single-pass transmembrane protein composed of a lumenal stress-sensing domain, and a cytosolic unit with a Ser/Thr kinase domain followed by an RNase domain. Both of the cytosolic domains are catalytically functional. In metazoans, IRE1α exerts most of its homeostatic effects by activating transcriptional programs via the ability of the RNase domain to regulate splicing of mRNA encoding the transcription factor XBP1 (Schröder and Kaufman, 2005; Ron and Walter, 2007). However, hexose-P mobilization and nucleotide sugar increases still occurred in ER-stressed XBP1$^{-/-}$ MEFs, although the TG responses were somewhat attenuated compared with DTT responses for reasons which remain unclear (Figures 8C and S4C). The absence of a requirement for XBP1 suggested two potential mechanisms for increasing hexose-Ps. As shown previously, it was possible that the IRE1α RNase domain caused degradation of a preexisting regulatory mRNA (Hollien and Weissman, 2006; Hetz and Glimcher, 2009). Such a mechanism might have degraded an mRNA involved in limiting glycogenolysis, causing elevation of hexose-P levels. Alternatively, IRE1α might have sent a signal directly from its kinase domain to stimulate glycogenolysis, without participation by the RNase domain.

To determine whether the entire cytosolic unit (kinase plus RNase domains) or the isolated kinase domain of IRE1α could activate glycogenolysis, we employed strategies used previously for expressing soluble fusions of the cytosolic units of yeast IRE (Aragon *et al.*, 2009) and mammalian IRE1α (Back *et al.*, 2006) to FKBP12-derived modules that bind the dimerizer AP20187 (Figure 9A). By dimerizing the fusion proteins, AP20187 promotes direct interaction of the attached domains and consequent activation of downstream events, including those possibly requiring transautophosphorylation. Rather than transient transfection (Back *et al.*, 2006), we prepared stable CHO-K1 transfectants to avoid contributions of hexose-Ps from untransfected cells in transiently transfected pools (Figure 9B). Thus, as for Figure 8B, we limited our analysis of these CHO-K1–derived lines to G6P.

In cells expressing the empty vector, AP20187 was inert as expected. However, in cells expressing the entire IRE1α cytosolic unit (kinase and RNase), AP20187 increased G6P (Figure 9C). This showed that IRE1α signaling is sufficient to mobilize hexose-P. As anticipated, cells expressing the kinase-only fusion protein failed to stimulate XBP1 splicing with AP20187 (Figure S5A). Yet, G6P in these cells was mobilized within 20 min of AP20187 addition at levels equivalent to those achieved with DTT-induced stress (Figure 9C). Preliminary experiments suggest this activity requires kinase function, because it was abrogated by a Lys^{599}Ala kinase-dead mutation, although the mutant protein was stably expressed. The effects of IRE1α activation were transient, suggesting a process for disengagement of signaling; after an initial increase, we detected a recovery phase within 1 h (Figure 9D). To verify that glycogenolysis was involved, we tested the GP inhibitor CP-91149. As shown in Figure 9E, CP-91149 blocked the AP20187-dependent increase of G6P in cells expressing the AP20187-responsive kinase domain. An extensive analysis of potential off-target effects of CP-91149 and AP20187 on reactions relevant to this study was performed (Figures S5B–F). Although some unanticipated effects of CP-91149 were identified, they did not affect the final outcomes of the experiments reported here. Moreover, there was no unexpected interference between CP-91149 and AP20187.

In summary, UPR signaling involving the IRE1α kinase domain activates glycogenolysis to elevate hexose-Ps. This allows IRE1α to regulate the ability of M6P to cause LLO destruction.

PERK stabilizes LLO pools despite ongoing LLO destruction

In general, the UPR plays an important role in maintaining ER homeostasis. Along these lines, the UPR can aid LLO assembly (Lehrman, 2006). One mechanism involves a role for PERK in balancing translation rates to compensate when LLO flux is impaired (Shang *et al.*, 2007; Figure 1). Additionally, since ER stress increased hexose-Ps, which are precursors of UDP-GlcNAc, GDP-mannose, and UDP-glucose, the nucleotide sugar building blocks for LLOs, we measured these molecules directly. As shown in Figure S4B, all three nucleotide sugars were increased by the UPR in an IRE1α-dependent manner, suggesting yet another mechanism by which the UPR may assist LLO assembly. LLO destruction by the UPR therefore presents a serious paradox. To address this problem, we hypothesized that suppression of LLO levels by a destructive mechanism in normal cells under conventional ER stress might be compensated by PERK, which can reduce LLO consumption by limiting *N*-glycoprotein synthesis (Figure 1).

Like PERK$^{-/-}$ MEFs, PERK$^{+/+}$ MEFs underwent LLO destruction in response to ER stress. Hexose-Ps, including M6P, were elevated (Figures 3B and 8C) and free glycans, resulting from LLO cleavage, were formed (Figure 5E). The other LLO cleavage product, Dol-P, appeared to be generated as well, although PERK's translation-attenuating activity predictably reduced the amount of Dol-P detected (Figures 2B,C). Free glycan formation in PERK$^{+/+}$ MEFs was also responsive to mannose treatment (Figure 7E). However, steady-state $G_3M_9Gn_2$-P-P-Dol levels were unaffected by either DTT or TG stress in PERK$^{+/+}$ MEFs (Figure 4B). In comparison, these stressors decreased LLO levels in PERK$^{-/-}$ MEFs by ~50%. This was attributable solely to differences in translation rate, because LLO levels in DTT-stressed PERK$^{-/-}$ MEFs were returned to normal by pharmacological rescue with the translation inhibitor CHX (Figure 10A).

These results demonstrate that translation attenuation by ER stress–activated PERK can ameliorate the effect of LLO destruction by stabilizing steady-state $G_3M_9Gn_2$-P-P-Dol levels. In this respect, the outcome of IRE1α/M6P signaling is antagonized by PERK. IRE1α/M6P signaling and LLO destruction themselves, however, are independent of PERK.

M6P signaling, LLO destruction, and LLO depletion during a pathogenic challenge with HSV-1

Since LLO destruction appeared benign in normal PERK-expressing cells under conventional ER stress with DTT or TG, we hypothesized

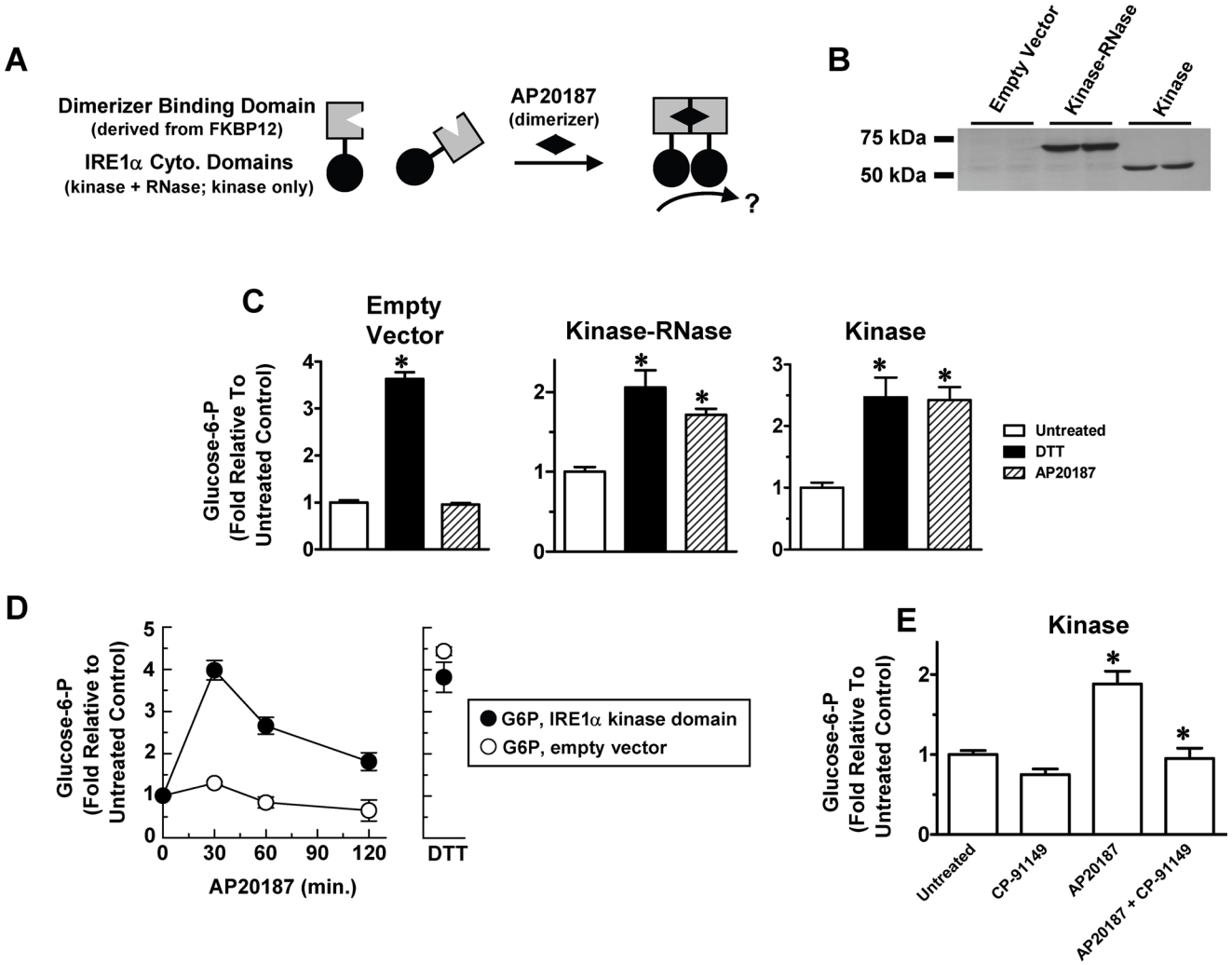

FIGURE 9: Inducible activation of the IRE1α kinase domain signals hexose-P mobilization. (A) AP20187 was used to dimerize the entire cytosolic unit of IRE1α (RNase + kinase domain) or the isolated kinase domain. (B) Immunoblots (anti-HA antibody) showing duplicate samples from stable CHO-K1 transfectants expressing the empty vector encoding FKBP12, or FKBP12 fusions with either the entire cytosolic unit or the kinase domain alone. (C) Cells were untreated (white bars), treated with 2 mM DTT for 1 h (black bars), or treated with 4 nM AP20187 for 20 min (hatched bars). G6P is expressed as fold change compared with untreated cells (mean ± SEM; *, $p < 0.0001$ for untreated controls compared with DTT-treated and AP20187-treated samples). Left, empty vector (n = 3); center, complete cytosolic unit (n = 4); right, kinase domain only (n = 7); (D) Time course of AP20187 treatment of empty vector (white symbols) or kinase domain only (black symbols) transfectants showing relative G6P expressed as fold increase compared with untreated cells (0 min). A 2 mM DTT, 60-min result in the same experiment is also shown. Points are averages of duplicates ± range. (E) G6P in "kinase domain only" transfectants, as in (C) after no treatment or treatments with 4 nM AP20187 for 20 min and/or 50 μM CP-91149 for 2 h (mean ± SEM; n = 12; *, $p < 0.0001$ for untreated controls compared with AP20187-treated samples, and for the latter compared with AP20187 + CP-91149-treated samples).

that a biological context for LLO destruction might involve an abnormal condition, where loss of LLOs could be advantageous. One such condition could be infection with a pathogen required to synthesize *N*-glycosylated components, a conjecture we chose to test with HSV-1, because this virus contains a number of envelope *N*-glycoproteins (Compton and Courtney, 1984, 1985). In addition, virally infected mammalian cells can attenuate translation to hinder synthesis of viral polypeptides and to initiate autophagy/xenophagy (Tallóczy *et al.*, 2002, 2006; Orvedahl *et al.*, 2007), but HSV-1 has developed countermeasures to prevent translation attenuation, including that dependent upon PERK (Mulvey *et al.*, 2007). This increased the likelihood that any LLO destruction induced by HSV-1–associated ER stress might also suppress LLO levels, as we observed in PERK knockout cells stressed with DTT and TG (Figures 4B and 10A).

Normal MEFs were mock-infected, infected with HSV-1 at saturating multiplicity, or TG-treated. Hexose-Ps, free glycans, and LLOs were then harvested. Shown in Figure 10B, G6P and M6P increased similarly after TG treatment and 12 h postinfection (h.p.i.) with HSV-1, which is indicative of ER stress caused by infection. LLO destruction occurred in both cases, resulting in an increased pool of qualitatively indistinguishable free glycans (Figure 10C). Importantly, normal MEFs under HSV-1–induced ER stress had LLO levels decreased by ~50% (Figure 10, B and D), similar to that observed with $PERK^{-/-}$ MEFs under conventional ER stress (Figure 4B). There was little effect at 5 h.p.i., when synthesis of a representative

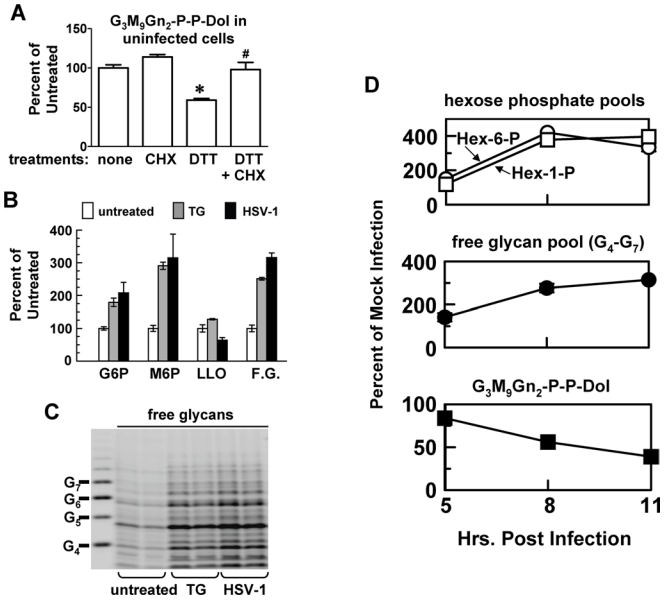

FIGURE 10: HSV-1 infection mobilizes M6P, with destruction and depletion of LLOs. (A) Uninfected PERK$^{-/-}$ MEFs were treated with 2 mM DTT and/or 0.2 mM CHX for 1 h, as indicated, and $G_3M_9Gn_2$-P-P-Dol was measured (n = 3, mean ± SEM). *, $p < 0.0001$ for untreated controls compared with DTT-treated samples; #, $p < 0.002$ for the latter compared with DTT + CHX-treated samples. (B) Normal (PERK$^{+/+}$) MEFs were stressed with TG (gray) or infected with HSV-1 (black). G6P, M6P, $G_3M_9Gn_2$-P-P-Dol LLO, and free glycans in the G_4–G_7 range (F.G.) are expressed as percentages of untreated cells (white), average of duplicates ± range. Cells were infected at multiplicity of infection (moi) = 7.5 and analyzed 12 h.p.i. (C) FACE gel showing free glycans associated with (B). (D) PERK$^{+/+}$ MEFs were infected as for (B). Total hexose-1-Ps (white squares), total hexose-6-Ps (white circles), free glycans in the G_4 -G_7 range (black circles), and $G_3M_9Gn_2$-P-P-Dol (black squares) are expressed as percentages of 5 h mock infection, averages of duplicates ± range (error bars are obscured by symbols).

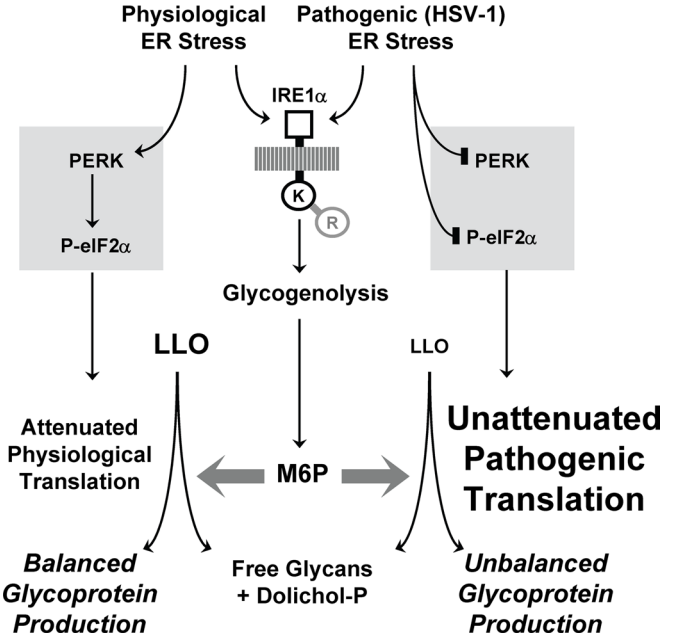

FIGURE 11: LLO destruction and depletion by M6P signaling during a pathogenic UPR. LLO destruction involves UPR signaling by the IRE1α kinase domain, and mobilization of M6P from glycogen. M6P then promotes LLO cleavage, yielding dolichol-P and lumenal free glycans, possibly by stimulating a hydrolytic activity of OT. PERK activation by conventional ER stress attenuates translation, and reduces LLO consumption for *N*-glycoprotein synthesis. This offsets the effect of the IRE1α signal for LLO destruction, which by itself is insufficient to suppress LLO levels. Thus, *N*-glycosylation of endogenous proteins remains balanced. In contrast, inhibition of PERK signaling to disable host defenses during HSV-1-induced stress removes the brake on *N*-glycoprotein synthesis, resulting in unabated LLO consumption. In combination with LLO destruction, this suppresses LLO levels, and envelope protein *N*-glycosylation becomes unbalanced. In this way, LLO destruction is not detrimental with conventional/physiological ER stresses, but may penalize invading pathogens for blocking translation-dependent host defenses.

glycoprotein (gC) was barely detectable (Figure S6A), but substantial effects were identified at 8–11 h.p.i. At this level of infection, when envelope glycoprotein synthesis was abundant, there was good temporal agreement between increases of M6P, increases of free glycans, and LLO loss (Figure 10D). To evaluate the plausibility of this approach for characterizing LLO destruction in the future with other enveloped viruses studied elsewhere, we demonstrated that results with HSV-1–infected MEFs prepared and analyzed in MAL's laboratory (Figure 10) were also observed with methanolic suspensions of HSV-1-infected MEFs prepared by IM's laboratory and shipped to the MAL's laboratory for analysis (Figure S6B). Taken together, we propose that viral infection is a biological context for M6P signaling and LLO destruction, possibly to suppress levels of LLOs required by the pathogen.

DISCUSSION

LLO destruction modifies the paradigm for protein *N*-glycosylation

The enigmatic ability of free M6P to promote cleavage of LLO molecules in permeabilized mammalian cells, reported earlier (Gao *et al.*, 2005), is shown here to represent the terminus of a signaling pathway for regulated LLO destruction. This pathway is triggered by ER stress, leading to a cascade of IRE1α kinase domain activation, enhanced glycogenolysis, and elevated M6P concentrations (Figure 11). Complementary approaches demonstrated that increased M6P is both necessary and sufficient for LLO destruction, which yielded Dol-P plus lumenal free glycans to indicate cleavage within the pyrophosphate linkage. With conventional ER stressors (DTT, TG) in normal MEFs, PERK's ability to attenuate translation stabilized LLO levels in spite of ongoing LLO destruction. In contrast, stresses that accompanied an absence of PERK function (i.e., in DTT/TG-treated MEFs lacking PERK, or in normal MEFs infected by HSV-1) not only activated this pathway, but also resulted in significant suppression of LLO levels. These studies were initiated to explore a possible role of M6P in CDG-Ia, and support the notion that both elevated M6P and diminished M1P may contribute synergistically to the etiology of this disease. This dual effect may explain the high frequency of its diagnosis, compared with all other forms of CDG. Together, our findings alter the broadly accepted paradigm for LLO synthesis and protein *N*-glycosylation to include unanticipated roles for regulated destruction of LLOs by M6P signaling.

Our results help explain recent results from experiments in which mannose metabolism was perturbed. In phosphomannose isomerase–deficient MEFs unable to interconvert M6P with F6P, incubation with 0.5 mM mannose medium significantly increased cellular M6P (Higashidani *et al.*, 2009). Interestingly, the M6P elevation was associated with decreased $G_3M_9Gn_2$-P-P-Dol, although Dol-P and free glycans were not measured. In a different approach,

mannosidase Man2C1, which catabolizes free cytosolic glycans to mannose, was overexpressed in HeLa cells (Bernon *et al.*, 2011). This maneuver also increased M6P, virtually eliminated $G_3M_9Gn_2$-P-P-Dol, and elevated free glycans having truncated LLO-type structures. Those authors concluded that the free glycans did not result from the type of LLO cleavage we reported with permeabilized cells (Gao *et al.*, 2005), because intact LLO-type glycans were detected in those earlier experiments. However, as we now report, LLO glycans released in ER-stressed intact cells become glycosidically degraded, and therefore appear consistent with glycans detected after Man2C1 overexpression. It still remains to be established whether the latter are lumenal or cytosolic.

Prior studies on saccharide metabolism in HSV-1–infected cells also agree well with the data presented in this paper. HSV-1 infection of human embryonic lung fibroblasts increased UDP-glucose (Brennan *et al.*, 1976), similar to results in Figures S4B and S6B. In addition, LLO levels were suppressed ~36% in HSV-1–infected African green monkey kidney (Vero) cells (Compton and Courtney, 1985), in accord with our measurements with MEFs (Figure 10, B and D). However, to our knowledge, this is the first study to report hexose-P increases during HSV-1 infection, and very little has been reported on this topic in virally infected cells.

M6P is a signaling molecule for an evolutionarily conserved process

M6P is the first small molecule reported to have a signaling role in the UPR, although other sugar phosphates can mediate signaling in unrelated pathways (Kabashima *et al.*, 2003). In this context, M6P appears to be acting similar to a second messenger. Its action involves amplifiable steps: M6P synthesis depends upon rapid enzymatic mobilization from a glycogen store, and it promotes an apparently catalytic process for LLO cleavage. Antagonism by the analogue M6Po suggests a defined target site. We have yet to demonstrate that M6P can be specifically inactivated to end signaling, a criterion for classical second-messenger action. However, if M6P has a special host-defense role in infected cells (see following section), it may be disadvantageous to terminate its action.

The M6P-activated enzyme remains unknown. OT is a strong candidate, because this enzyme naturally recognizes $G_3M_9Gn_2$-P-P-Dol, is less efficient with smaller LLO intermediates, and normally cleaves LLO at a slow basal rate in a process known as "transfer to water" (Turco *et al.*, 1977; Kelleher *et al.*, 2003; Gao *et al.*, 2005). Unfortunately, enriched OT preparations cannot be properly evaluated, because M6P-dependent LLO cleavage requires intact ER structure preserved by SLO-permeabilization (Gao *et al.*, 2005). M6P does not penetrate the ER of hepatocytes (Arion, 1989), which are capable of M6P-dependent LLO cleavage (Gao *et al.*, 2005). We therefore suggest that M6P might interact with an ER component having cytosolic elements, possibly one of the cytosolic domains of OT itself. Although little is known about the functions of OT's cytosolic sequences, one possible regulatory role has been reported for the *Saccharomyces cerevisiae* enzyme (Chavan *et al.*, 2003). It also remains to be determined whether LLO destruction could be carried out specifically by one of the two functionally distinct isoforms of OT (Ruiz-Canada *et al.*, 2009).

The bacterium *Campylobacter jejuni*, like eukaryotes, possesses an *N*-glycosylation pathway. It was recently shown that LLO destruction also occurs in this bacterium in response to hypoosmotic conditions (Nothaft *et al.*, 2009). Although the signaling pathway was not elucidated, release of bacterial oligosaccharides required OT activity, and was proposed to regulate periplasmic volume in response to osmotic changes. This suggests that LLO destruction may be an evolutionarily conserved response to environmental stress in multiple kingdoms of life.

A new signaling role for the IRE1 kinase domain—exacerbation of LLO imbalance

Although RNase activity is important in most IRE1α signaling, our data reveal additional RNase-independent signaling by the kinase domain, as have other studies (Lipson *et al.*, 2006). In particular, the "IREα interactome" mediates a number of scaffold activities of the autophosphorylated kinase domain that are important for apoptosis and autophagy (Hetz and Glimcher, 2009). Presently, the only known kinase substrate of IRE1α is itself. Our preliminary results suggest kinase function is required for IRE1α stimulation of glycogenolysis, a process clearly sensitive to phosphorylation (Johnson, 1992). Phospho-IRE1α, or a downstream relay, might conceivably phosphorylate a glycogenolysis factor. Since chronic ER stress is associated with obesity and insulin resistance (Özcan *et al.*, 2004), and glycogen metabolism is an important factor in glycemic control, our results suggest a new mode of involvement for IRE1α in these conditions.

At first glance, LLO destruction by conventional/physiological ER stress seems counterintuitive, because LLOs are required for *N*-glycosylation. However, LLO levels were suppressed by LLO destruction only when PERK function was impaired, such as by PERK knockout or infection by HSV-1. This pathogen interferes with PERK signaling to impair xenophagy and maximize production of envelope proteins, which require LLOs. Thus HSV-1 disables the brake that would otherwise match protein synthesis to LLO amount (Figure 1). As we showed previously, *N*-glycoprotein synthesis without this brake becomes unbalanced, and LLO need can outpace supply (Shang *et al.*, 2007). In support of this concept, envelope glycoproteins gB and gC in HSV-1–infected Vero and HEp-2 cells were underglycosylated (Compton and Courtney, 1984). In our study, gC in lysates of HSV-1–infected MEFs was also underglycosylated (Figure S6C). We suggest that LLO destruction signaled by IRE1's kinase domain functions to exacerbate the LLO imbalance caused by unabated viral polypeptide production, resulting in suppression of LLO levels and underglycosylation of viral polypeptides (Figure 11).

In this respect, LLO destruction could be an "arms race" mechanism to specifically penalize pathogens that interfere with host defenses involving PERK and eIF2α signaling (Tallóczy *et al.*, 2002; Mulvey *et al.*, 2007). The apparent futility of M6P causing destruction of its downstream LLO product may therefore be an advantage. Since it is used for synthesis of the LLO precursor GDP-mannose, M6P may be pathogen-proof, as pathogens with *N*-glycosylated components would suffer if they caused M6P loss. To evaluate such hypotheses, interference with either IRE1α or GP are unattractive experimental options, due to complicating pleiotropic effects. Rather, we envision experiments that interfere directly with LLO destruction, with the predicted result of more highly glycosylated virus populations with the potential to influence virulence and/or pathogenesis. It would also be fruitful to screen for viruses that have devised mechanisms to disable the LLO destruction reaction.

MATERIALS AND METHODS

Reagents

We received at no cost CP-91149 from Pfizer (Groton, CT), and AP20187 and ARGENT vectors from Ariad Pharmaceuticals (Cambridge, MA). TN, TG, DTT, CHX, 1,4-dideoxy-1,4-imino-D-arabinitol, caffeine, M6P, G6P, F6P, G1P, M1P, and mannose (all hexoses in D configuration) were from Sigma-Aldrich (St. Louis, MO). z-VAK-fmk was from Promega (Madison, WI). Control and acceptor tripeptides

for OT were designed and synthesized by SynPep (Dublin, CA) as previously described (Gao and Lehrman, 2002b). ANDS and AMAC were from Molecular Probes/Invitrogen (Carlsbad, CA), and all other FACE supplies were obtained as previously described (Gao and Lehrman, 2002a). Endoglycosidase H was from Calbiochem (San Diego, CA), and jack bean α-mannosidase was from Glyko/Prozyme (Hayward, CA). SLO was from Corgenix (Broomfield, CO). Radiolabeled compounds were UDP-[^{3}H]GlcNAc (36 Ci/mmol; DuPont, Wilmington, DE), GDP-[^{3}H]mannose (15 Ci/mmol; American Radiolabeled Chemicals, St. Louis, MO), [^{3}H]inulin (510 mCi/mmol; Amersham, GE Healthcare, Waukesha, WI), and [^{14}C]urea (59 mCi/mmol; Amersham). Anti-HA (#2999), anti-PERK (#3192), anti-GAPDH (#3683), anti–phospho-eIF2α (#9721), and anti-IRE1α (#3294) were from Cell Signaling Technology (Danvers, MA). Anti–HSV-1 gC (#NB110-57251) was from Novus Biologicals (Littleton, CO). Antitubulin was a gift of Melanie Cobb (University of Texas Southwestern Medical Center at Dallas).

Cell cultures

Cell culture media were from Invitrogen and sera were from Atlanta Biologicals (Norcross, GA). CHO-K1 (Camp *et al.*, 1993), GRP78/BiP-overexpressing CHO-K1 transfectants (Dorner *et al.*, 1992), and Fv2E-PERK-expressing CHO-K1 transfectants (Lu *et al.*, 2004) were grown in Ham's F-12 plus 10% fetal bovine serum (FBS) without antibiotics. Various control and knockout mouse embryonic fibroblasts (PERK$^{+/+}$ and PERK$^{-/-}$ [Harding *et al.*, 2000]); IRE1α$^{+/+}$ and IRE1α$^{-/-}$ [Urano *et al.*, 2000]; XBP1$^{+/+}$ and XBP1$^{-/-}$ [Lee *et al.*, 2003]; and MPI$^{+/+}$ [DeRossi *et al.*, 2006]) were cultured in RPMI 1640 medium plus 10% FBS without antibiotics, unless indicated otherwise. However, all siRNA incubations used DMEM plus 10% FBS for more optimal knock-down. Gelatin-coated dishes were used for all cells in experiments involving PERK$^{-/-}$ MEFs treated with DTT or TG, which was necessary to maintain good adhesion of these cells when under ER stress (Shang *et al.*, 2007). Phenotypes of MEF lines with homozygous disruptions of the PERK and IRE1α genes were independently verified by the lack of immunologically detectable PERK or IRE1α, and the absence of stress-dependent formation of P-eIF2α or spliced XBP1 mRNA, respectively.

FACE analyses of LLO glycans, free glycans, nucleotide sugars, and monosaccharide phosphates

Published methods were followed (Gao and Lehrman, 2002a, 2003, 2006). Briefly, LLOs were recovered in chloroform:methanol:water (10:10:3) extracts, after which glycans were released with mild acid. Free glycans, monosaccharide phosphates, and nucleotide sugars (eventually yielding free neutral hexoses) were recovered in aqueous extracts, and separated by anion exchange. Hexose-1-phosphates and nucleotide sugars were then selectively hydrolyzed to neutral hexoses, leaving hexose-6-phosphates unaffected. Glycans were conjugated with ANDS and separated with oligosaccharide profiling gels, while neutral hexoses and hexose-6-Ps were conjugated with AMAC and resolved with monosaccharide profiling (borate) gels. Where indicated, ANDS-conjugated glycans were digested with endoglycosidase H or jack bean α-mannosidase prior to electrophoresis. Per 10^7 cells, 5% of the sample for monosaccharide analysis, and 50% of the sample for glycan analysis, was usually loaded per gel lane.

For FACE data analysis, gel images were acquired with a Bio-Rad Fluor-S MultiImager using a 530DF60 filter (Hercules, CA). When necessary, individual bands of ANDS and AMAC conjugates on gels were located and quantified with Quantity One software supplied with the scanner. Alternatively, entire pools of ANDS-conjugated free glycans migrating in the G_4–G_7 standard range were quantified as a group. For clarity, some images were adjusted with brightness and contrast tools in Microsoft PowerPoint 2003 (Redmond, WA), treating all data from a single gel identically. In some cases, irrelevant lanes were removed by cropping and joining. In many experiments, we only compared samples loaded on the same FACE gel, often limiting the experiments to duplicate determinations, and we therefore present original FACE images and/or means ± error ranges. In experiments with at least three determinations, we report means ± SEM and also p values from two-tailed *t* tests determined with Graphpad Prism 5 software (La Jolla, CA).

SLO-permeabilized cells

For assessment of Dol-P, monolayers were permeabilized with SLO after the indicated treatments and incubated at 37°C for 20 min with 2 ml transport buffer containing 0.1 μCi UDP-[^{3}H]GlcNAc or 0.2 μCi GDP-[^{3}H]mannose, and 2 mM AMP. Where indicated, 50 μM "control" (Ac-Gln-Tyr-Thr-$CONH_2$) or "acceptor" (Ac-Asn-Tyr-Thr-$CONH_2$) tripeptides for OT were included. [^{3}H]lipids were recovered by extraction with chloroform:methanol (2:1) with aqueous back-washing, evaporated to dryness, and measured by liquid scintillation spectroscopy (Gao and Lehrman, 2002b). Since our ability to achieve consistent permeabilization across multiple samples in a single experiment was hindered by handling excessive numbers of dishes, it was necessary to limit most treatments to duplicates, in which case we report averages and variance where appropriate.

For separation of lumenal and cytosolic free glycans, cells were permeabilized with SLO, but glycosyltransferase substrates were omitted from the transport buffer. Incubations were for 4 min at 37°C, followed by 15 min on ice.

SLO-permeabilized cells were also used for in vitro LLO cleavage assays with M6P (Gao *et al.*, 2005). In addition to the indicated monosaccharides, the reactions (1 h 37°C) included 100 μM UDP-GlcNAc, 200 μM UDP-glucose, and 0.2 μM GDP-mannose to generate LLOs, and 5 μg/ml each of castanospermine and deoxymannojirimycin to inhibit glycosidases.

RNA interference of IRE1α in MEFs

Mouse (NM_023913) ERN1 ON-TARGETplus SMART Pool (L-041030-00-0005) containing four siRNA duplexes targeting GAAAGGUGGUGCACAUCAA (siRNA1); CGUCAUUGCUCGUGAAUUG (siRNA2); UGAACUACUUGAGGAAUUA (siRNA3), and UGACGAAACUUCCCUUUAC (siRNA4) were from Dharmacon (Thermo Fisher Scientific, Lafayette, CO). RNA interference was carried out with Lipofectamine RNAiMAX Transfection Reagent (Invitrogen) according to the manufacturer's instructions, with modifications. Buffer alone or with siRNAs was mixed with ~10^6 trypsinized MEFs in 100-mm dishes to reach 10 nM siRNA and achieve 30–40% confluence the next day. Cells were passaged 48 h later to 100-mm dishes and grown in siRNA-free media for at least 24 h to achieve 80–90% of confluence. Cells were fed fresh medium at least 1 h prior to receiving additional treatments.

AP20187-responsive ARGENT constructs for IRE1α kinase domain only (aa 468–836) or cytosolic unit (kinase ± RNase domain; aa 468–977)

Two micrograms total MEF RNA was used for first-strand cDNA synthesis with SuperScript First-Strand Synthesis System for RT-PCR (#1904-018; Invitrogen). Of the cDNA, 10% was used to amplify IRE1α inserts with Expand High Fidelity^{plus} PCR System (#03300242001; Roche, Indianapolis, IN) with the primer pairs (based upon Back *et al.* [2006] and NM_023913; *Spe*I sites

underlined in primers listed below): 5′-TTTCCTACTAGTCTGAGCGTGCATCAGCAG-3′ (forward for both constructs) and either 5′-TTTCCTACTAGTCTCCAGGCTCCAGAAGAAGG-3′ (reverse for kinase plus RNase) or 5′-TTTCCTACTAGTGAGGGCATATGGAATCACTG-3′ (reverse for kinase only). Both cDNA fragments were ligated (Rapid DNA Ligation Kit, #11635379001; Roche) into *Spe*I-digested pC_4-F_v1E (a kind gift from Ariad Pharmaceuticals) and transformed into *Escherichia coli*. Plasmid inserts were screened by *Spe*I digestion, and orientations were verified by both *Xho*I digestion and DNA sequencing. Spurious point mutations were corrected with the QuikChange II Site-Directed Mutagenesis Kit (#200523; Stratagene, Agilent Technologies, Santa Clara, California) and resequenced. Plasmids preparation, PCR product purification, and DNA digest extraction were done with Qiagen products (Valencia, CA): Spin Miniprep Kit, PCR Purification Kit, and Gel Extraction Kit.

Selection of stable transfectants

Plasmids encoding the kinase domain only (designated pC_4F_v-1E-K, abbreviated pK) or the kinase plus RNase domain (pC_4F_v-1E-K+R, pK+R), or the empty vector pC_4F_v-1E were cotransfected in 10-fold excess with plasmid pMAM-neo for stable selection into CHO-K1 cells with FuGENE HD Transfection Reagent (#04709691001; Roche). Well-separated single colonies were picked with cloning cylinders after selection with 800 μg/ml G418. Colonies were screened for relative expression levels and sizes of IRE1α fusion proteins by immunoblotting detergent extracts with anti-HA antibody to detect the HA epitope tag fused to the C-termini of the encoded proteins by the pC_4F_v-1E vector. The colonies with highest expression levels of kinase only or kinase plus RNase fusion proteins were designated pK5 and pK+R11, respectively, and were used in all experiments presented here (a pK sibling transfectant with fivefold lower levels of fusion protein than pK5 gave a similar response to AP20187, as in Figure 9C).

Immunoblotting

Cells grown in 100-mm dishes were lysed with 0.3–0.4 ml RIPA buffer (150 mM sodium chloride, 1.0% NP-40, 0.5% sodium deoxycholate, 0.1% SDS, 50 mM Tris, pH 8.0) supplemented with protease inhibitors (Complete Mini Protease Inhibitor Cocktail Tablets, #11836153001; Roche) and phosphatase inhibitors (PhosSTOP, Phosphatase Inhibitor Cocktail Tablets, #04906837001; Roche), one tablet each per 10 ml buffer. After vortexing, lysates were kept on ice for 30 min, then clarified by centrifugation. Protein was measured with a BCA protein assay kit (#23225; Pierce, Thermo Fisher Scientific, Rockford, IL). Lysate protein (15–40 μg) was subjected to SDS–PAGE with single acrylamide concentrations from 6–10%. Proteins were transferred to Protran nitrocellulose membrane (Whatman, Piscataway, NJ), blocked with Tris-buffered saline (TBS)-T (20 mM Tris-Cl, pH 7.6, 137 mM NaCl, 0.1% Tween-20) containing 5% nonfat milk, and probed with antibodies prediluted in TBS-T containing 5% bovine serum albumin (BSA; #001-000-162; Jackson ImmunoResearch Laboratories, West Grove, PA) with overnight incubation at 4°C. Target proteins were detected with Amersham ECL Western Blotting Detection Reagents (#RPN2109, Amersham, GE Healthcare) and visualized by exposure to X-ray film, scanning with a Bio-Rad Fluor-S MultiImager, and processing with Bio-Rad Quantity-One software.

XBP1 Splicing

Total mRNA (RNeasy; Qiagen, Valencia, CA) isolated after the indicated treatment was used for a PCR-based assay to assess XBP1 mRNA splicing (Shang and Lehrman, 2004). PCR products representing spliced XBP1, unspliced XBP1, and a hybrid formed during the chain reaction (denoted with the subscripts S, U, and H, respectively) were resolved by agarose gel electrophoresis.

Measurement of cellular mannosyl phosphate concentrations

Cellular concentrations of M6P were determined in $PERK^{-/-}$ MEFs after quantification from known cell numbers by FACE, and measurement of cellular volume by the [^{3}H]inulin-[^{14}C]urea method (Oehler *et al.*, 1996).

HSV-1 methods

HSV-1 strain 17 and Vero cells were obtained from Beth Levine (University of Texas Southwestern Medical Center at Dallas). Virus was propagated and high-titer stocks were prepared with Vero cells (cultured in DMEM plus 10% FBS) by standard procedures. Titers were determined by serial dilution in plaque assays. Infections of MEFs (cultured with RPMI 1640) were initiated with monolayers at ~90% confluence with virus at a multiplicity of 7.5–10, as indicated, over a period of 1 h at 37°C with medium containing 2% heat-inactivated FBS. Infections were then continued by changing to medium with 10% heat-inactivated FBS. Cells were inspected for cytopathic effect 5 h after infection to ensure that the vast majority of cells were infected. All virus infections included 50 μg/ml gentamicin.

ACKNOWLEDGMENTS

This work is supported by NIH grants DK-042394, HL-052173, and HL-057346 to R.J.K.; by NIH grants AI-073898 and GM-056927 to I.M.; by NIH grant R-37-DK047119 and a Principal Research Fellowship from the Wellcome Trust to D.R.; by NIH grant GM-031278 and support from the Robert Welch Foundation to J.R.F.; and by NIH grant GM-038545 and Robert Welch Foundation grant I-1168 to M.A.L. We gratefully acknowledge Pfizer for CP-91149 and Ariad Pharmaceuticals for AP20187 and ARGENT vectors. We thank Laurie Glimcher for $XBP1^{+/+}$ and $XBP1^{-/-}$ MEFs, Beth Levine and members of her laboratory for instruction on the handling and use of HSV-1, Judith Treadway of Pfizer for advice on GP inhibitors, and Thomas Rutkowski and Joseph Contessa for highly useful comments on the manuscript.

REFERENCES

Aragon T, van Anken E, Pincus D, Serafimova IM, Korennykh AV, Rubio CA, Walter P (2009). Messenger RNA targeting to endoplasmic reticulum stress signalling sites. Nature 457, 736–740.

Arion WJ (1989). Measurement of intactness of rat liver endoplasmic reticulum. Methods Enzymol 174, 58–67.

Back SH, Lee K, Vink E, Kaufman RJ (2006). Cytoplasmic IRE1-α-mediated XBP1 mRNA splicing in the absence of nuclear processing and endoplasmic reticulum stress. J Biol Chem 281, 18691–18706.

Belakhov V, Dovgolevsky E, Rabkin E, Shulami S, Shoham Y, Baasov T (2004). Synthesis and evaluation of a mechanism-based inhibitor of KDO8P synthase. Carbohydr Res 339, 385–392.

Bernon C *et al.* (2011). Overexpression of Man2C1 leads to protein underglycosylation and upregulation of ERAD pathway. Glycobiology 21, 363–375.

Brennan PJ, Steiner SM, Courtney RJ, Skelly J (1976). Metabolism of galactose in herpes simplex virus-infected cells. Virology 69, 216–228.

Camp LA, Chauhan P, Farrar JD, Lehrman MA (1993). Defective mannosylation of glycosylphosphatidylinositol in Lec35 Chinese hamster ovary cells. J Biol Chem 268, 6721–6728.

Chantret I, Moore SEH (2008). Free oligosaccharide regulation during mammalian protein N-glycosylation. Glycobiology 18, 210–224.

Chavan M, Rekowicz M, Lennarz W (2003). Insight into functional aspects of Stt3p, a subunit of the oligosaccharyl transferase. J Biol Chem 278, 51441–51447.

Compton T, Courtney RJ (1984). Evidence for post-translational glycosylation of a nonglycosylated precursor protein of herpes simplex virus type 1. J Virol 52, 630–637.

Compton T, Courtney RJ (1985). Effect of herpes simplex virus type 1 on cellular pools of oligosaccharide-lipid. Virology 147, 1–8.

DeRossi C, Bode L, Eklund EA, Zhang F, Davis JA, Westphal V, Wang L, Borowsky AD, Freeze HH (2006). Ablation of mouse phosphomannose isomerase (Mpi) causes mannose-6-phosphate accumulation, toxicity, and embryonic lethality. J Biol Chem 281, 5916–5927.

Doerrler WT, Lehrman MA (1999). Regulation of the dolichol pathway in human fibroblasts by the endoplasmic reticulum unfolded protein response. Proc Natl Acad Sci USA 96, 13050–13055.
Dorner AJ, Wasley LC, Kaufman RJ (1992). Overexpression of GRP78 mitigates stress induction of glucose regulated proteins and blocks secretion of selective proteins in Chinese hamster ovary cells. EMBO J 11, 1563–1571.
Gao N, Lehrman MA (2002a). Analyses of dolichol pyrophosphate-linked oligosaccharides in cell cultures and tissues by fluorophore-assisted carbohydrate electrophoresis. Glycobiology 12, 353–360.
Gao N, Lehrman MA (2002b). Coupling of the dolichol-P-P-oligosaccharide pathway to translation by perturbation-sensitive regulation of the initiating enzyme, GlcNAc-1-P transferase. J Biol Chem 277, 39425–39435.
Gao N, Lehrman MA (2003). Letter to the Glycoforum: Alternative sources of reagents and supplies for fluorophore-assisted carbohydrate electrophoresis (FACE). Glycobiology 13, 1G–3G.
Gao N, Lehrman MA (2006). Non-radioactive analysis of lipid-linked oligosaccharide compositions by fluorophore-assisted carbohydrate electrophoresis (FACE). Methods Enzymol 415, 3–20.
Gao N, Shang J, Lehrman MA (2005). Analysis of glycosylation in CDG-Ia fibroblasts by fluorophore-assisted carbohydrate electrophoresis: implications for extracellular glucose and intracellular mannose-6-phosphate. J Biol Chem 280, 17901–17909.
Gill A, Gao N, Lehrman MA (2002). Rapid activation of glycogen phosphorylase by the endoplasmic reticulum unfolded protein response. J Biol Chem 277, 44747–44753.
Grant SR, Lennarz WJ (1983). Relationship between oligosaccharide-lipid synthesis and protein synthesis in mouse LM cells. Eur J Biochem 134, 575–583.
Harding HP, Zhang Y, Bertolotti A, Zeng H, Ron D (2000). *Perk* is essential for translational regulation and cell survival during the unfolded protein response. Mol Cell 5, 897–904.
Hetz C, Glimcher LH (2009). Fine-tuning of the unfolded protein response: assembling the IRE1α interactome. Mol Cell 35, 551–561.
Higashidani A, Bode L, Nishikawa A, Freeze HH (2009). Exogenous mannose does not raise steady state mannose-6-phosphate pools of normal or *N*-glycosylation-deficient human fibroblasts. Mol Genet Metab 96, 268–272.
Hollien J, Weissman JS (2006). Decay of endoplasmic reticulum-localized mRNAs during the unfolded protein response. Science 313, 104–107.
Hubbard SC, Robbins PW (1980). Synthesis of the *N*-linked oligosaccharides of glycoproteins. J Biol Chem 255, 11782–11789.
Jaeken J, Matthijs G (2001). Congenital disorders of glycosylation. Annu Rev Genomics Hum Genet 2, 129–151.
Johnson LN (1992). Glycogen phosphorylase: control by phosphorylation and allosteric effects. FASEB J 6, 2274–2282.
Kabashima T, Kawaguchi T, Uyeda K (2003). Xylulose 5-phosphate mediates glucose-induced lipogenesis by xylulose 5-phosphate-activated protein phosphatase in rat liver. Proc Natl Acad Sci USA 100, 5107–5112.
Kelleher DJ, Karaoglu D, Mandon EC, Gilmore R (2003). Oligosaccharyltransferase isoforms that contain different catalytic STT3 subunits have distinct enzymatic properties. Mol Cell 12, 101–111.
Kornfeld R, Kornfeld S (1985). Assembly of asparagine-linked oligosaccharides. Annu Rev Biochem 54, 631–664.
Lee AH, Iwakoshi NN, Glimcher LH (2003). XBP-1 regulates a subset of endoplasmic reticulum resident chaperone genes in the unfolded protein response. Mol Cell Biol 23, 7448–7459.
Lehrman MA (1991). Biosynthesis of *N*-Acetylglucosamine-P-P-dolichol, the committed step of asparagine-linked oligosaccharide assembly. Glycobiology 1, 553-562.
Lehrman MA (2006). Stimulation of N-linked glycosylation and lipid-linked oligosaccharide synthesis by stress responses in metazoan cells. Crit Rev Biochem Mol Biol 41, 51–75.
Lehrman MA (2007). Teaching dolichol-linked oligosaccharides more tricks with alternatives to metabolic radiolabeling. Glycobiology 17, 75R–85R.
Levine AJ, Puzio-Kuter AM (2010). The control of the metabolic switch in cancers by oncogenes and tumor suppressor genes. Science 330, 1340–1344.
Lipson KL, Fonseca SG, Ishigaki S, Nguyen LX, Foss E, Bortell R, Rossini AA, Urano F (2006). Regulation of insulin biosynthesis in pancreatic beta cells by an endoplasmic reticulum-resident protein kinase IRE1. Cell Metab 4, 245–254.
Lu PD, Harding HP, Ron D (2004). Translation reinitiation at alternative open reading frames regulates gene expression in an integrated stress response. J Cell Biol 167, 27–33.
Marquardt T, Freeze H (2001). Congenital disorders of glycosylation: glycosylation defects in man and biological models for their study. Biol Chem 382, 161–177.
Martin WH, Hoover DJ, Armento SJ, Stock IA, McPherson RK, Danley DE, Stevenson RW, Barrett EJ, Treadway JL (1998). Discovery of a human liver glycogen phosphorylase inhibitor that lowers blood glucose in vivo. Proc Natl Acad Sci USA 95, 1176–1181.
Misaghi S, Pacold ME, Blom D, Ploegh HL, Korbel GA (2004). Using a small molecule inhibitor of peptide: N-glycanase to probe its role in glycoprotein turnover. Chem Biol 11, 1677–1687.
Moore SEH, Bauvy C, Codogno P (1995). Endoplasmic reticulum-to-cytosol transport of free polymannose oligosaccharides in permeabilized HepG2 cells. EMBO J 14, 6034-6042.
Mulvey M, Arias C, Mohr I (2007). Maintenance of endoplasmic reticulum (ER) homeostasis in herpes simplex virus type 1-infected cells through the association of a viral glycoprotein with PERK, a cellular ER stress sensor. J Virol 81, 3377–3390.
Nothaft H, Liu X, McNally DJ, Li J, Szymanski CM (2009). Study of free oligosaccharides derived from the bacterial *N*-glycosylation pathway. Proc Natl Acad Sci USA 106, 15019–15024.
Oehler R, Hefel B, Roth E (1996). Determination of cell volume changes by an inulin-urea assay in 96-well plates: A comparison with Coulter counter analysis. Anal Biochem 241, 269–271.
Oikonomakos NG, Skamnaki VT, Tsitsanou KE, Gavalas G, Johnson LN (2000). A new allosteric site in glycogen phosphorylase b as a target for drug interactions. Structure 8, 575–584.
Oikonomakos NG, Tiraidis C, Leonidas DD, Zographos SE, Kristiansen M, Jessen CU, Norskov-Lauritsen L, Agius L (2006). Iminosugars as potential inhibitors of glycogenolysis: structural insights into the molecular basis of glycogen phosphorylase inhibition. J Med Chem 49, 5687–5701.
Orvedahl A, Alexander D, Tallóczy Z, Sun Q, Wei Y, Zhang W, Burns D, Leib DA, Levine B (2007). HSV-1 ICP34.5 confers neurovirulence by targeting the beclin 1 autophagy protein. Cell Host Microbe 1, 23–35.
Özcan U, Cao Q, Yilmaz E, Lee AH, Iwakoshi NN, Ozdelen E, Tuncman G, Gorgun C, Glimcher LH, Hotamisligil GS (2004). Endoplasmic reticulum stress links obesity, insulin action, and type 2 diabetes. Science 306, 457–461.
Rath VL *et al.* (2000). Human liver glycogen phosphorylase inhibitors bind at a new allosteric site. Chem Biol 7, 677–682.
Ron D, Walter P (2007). Signal integration in the endoplasmic reticulum unfolded protein response. Nat Rev Mol Cell Biol 8, 519–529.
Ruiz-Canada C, Kelleher DJ, Gilmore R (2009). Cotranslational and post-translational *N*-glycosylation of polypeptides by distinct mammalian OST isoforms. Cell 136, 272–283.
Schenk B, Fernandez F, Waechter CJ (2001). The ins(ide) and outs(ide) of dolichyl phosphate biosynthesis and recycling in the endoplasmic reticulum. Glycobiology 11, 61R–70R.
Schmitt JW, Elbein AD (1979). Inhibition of protein synthesis also inhibits synthesis of lipid-linked oligosaccharides. J Biol Chem 254, 12291–12294.
Schröder M, Kaufman RJ (2005). The mammalian unfolded protein response. Annu Rev Biochem 74, 739–789.
Shang J, Gao N, Kaufman RJ, Ron D, Harding HP, Lehrman MA (2007). Translational balancing by the eIF2α kinase PERK couples ER glycoprotein synthesis to lipid-linked oligosaccharide flux. J Cell Biol 176, 605–616.
Shang J, Lehrman MA (2004). Discordance of UPR signaling by ATF6 and Ire1p-XBP1 with levels of target transcripts. Biochem Biophys Res Commun 317, 390–396.
Sood R, Porter AC, Ma K, Quilliam LA, Wek RC (2000). Pancreatic eukaryotic initiation factor-2α kinase (PEK) homologues in humans, *Drosophila melanogaster* and *Caenorhabditis elegans* that mediate translational control in response to endoplasmic reticulum stress. Biochem J 346, 281–293.
Spiro MJ, Spiro RG, Bhoyroo VD (1976). Lipid-saccharide intermediates in glycoprotein biosynthesis: I. Formation of an oligosaccharide-lipid by thyroid slices and evaluation of its role in protein glycosylation. J Biol Chem 251, 6400-6408.
Tallóczy Z, Jiang W, Virgin HW IV, Leib DA, Scheuner D, Kaufman RJ, Eskelinen EL, Levine B (2002). Regulation of starvation- and virus-induced autophagy by the eIF2alpha kinase signaling pathway. Proc Natl Acad Sci USA 99, 190–195.
Tallóczy Z, Virgin HW IV, Levine B (2006). PKR-dependent autophagic degradation of herpes simplex virus type 1. Autophagy 2, 24–29.
Turco SJ, Stetson B, Robbins PW (1977). Comparative rates of transfer of lipid-linked oligosaccharides to endogenous glycoprotein acceptors in vitro. Proc Natl Acad Sci USA 74, 4411–4414.
Urano F, Wang X-C, Bertolotti A, Zhang Y, Chung P, Harding HP, Ron D (2000). Coupling of stress in the ER to activation of JNK protein kinases by transmembrane protein kinase IRE1. Science 287, 664–666.